STRUCTURAL RELIABILITY: A PROCESSING DEPENDENT PHENOMENON

Evans, A.G.

1981-05-01

LBL-12208 c.2
Preprint

**Lawrence Berkeley Laboratory**
UNIVERSITY OF CALIFORNIA

## Materials & Molecular Research Division

Submitted to the Journal of the American Ceramic Society

# STRUCTURAL RELIABILITY:
# A PROCESSING DEPENDENT PHENOMENON

A.G. Evans

May 1981

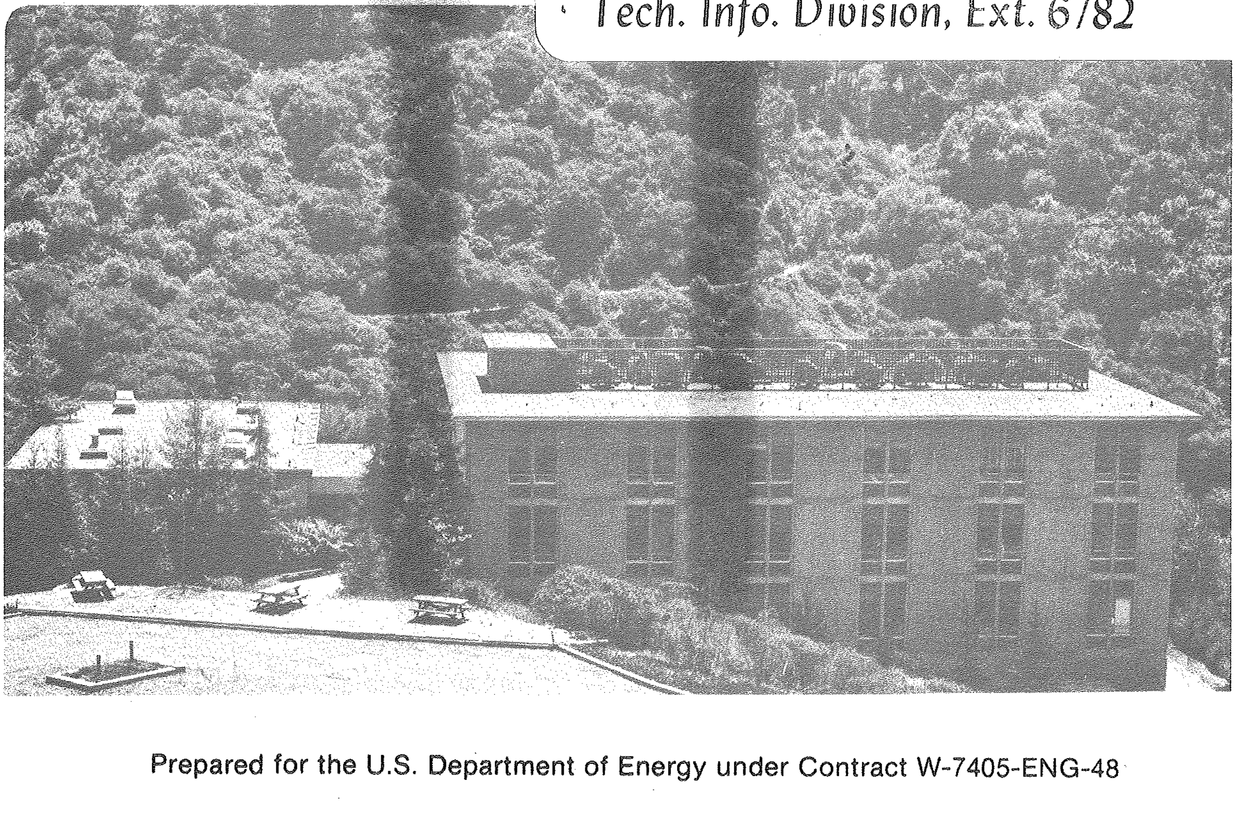

Prepared for the U.S. Department of Energy under Contract W-7405-ENG-48

# STRUCTURAL RELIABILITY:
# A PROCESSING DEPENDENT PHENOMENON

by

A. G. Evans

Materials and Molecular Research Division, Lawrence Berkeley Laboratory
and Department of Materials Science and Mineral
Engineering, University of California
Berkeley, CA 94720

## ABSTRACT

The principal sources of fracture in ceramic polycrystals have been identified. These include surface cracks, produced during surface finishing, and voids, inclusions or large grains generated during processing. The dominance of a specific fracture source depends upon the microstructure, the test temperature, and the stress distribution. The origins of processing induced defects have been examined, and certain dominant processing variables identified. Connections between processing and structural reliability have, thereby, been established.

This work was supported by the Director, Office of Energy Research, Office of Basic Energy Sciences, Materials Science Division of the U.S. Department of Energy under Contract No. W-7405-ENG-48 and by the U.S. Office of Naval Research, under Contract No. N00014-79-C-0159.

## 1. INTRODUCTION

The mechanical failure of ceramics occurs from defects. The defects are introduced during either fabrication or surface preparation (pre-existent flaws) or during exposure to aggressive environments (e.g. oxidation, projectile impact). Failure studies reveal an appreciable sensitivity of the failure condition to the defect type[1] (fig. 1) and to the surrounding microstructure.[2] Processing thus exerts an essential influence on structural reliability, as expressed through relations between the processing procedure, the defect population and microstructure of the material. The important fracture inducing defects can be characterized by pertinent non-destructive measurements (e.g. acoustic waves)[3]. Non-destructive techniques thus contribute importantly to the assurance of structural reliability, based upon an ability to reject defective components. The ultimate reliability of ceramic components must be based on the appropriate combination of processing controls and non-destructive measurement procedures suggested by a comprehensive fundamental understanding of fracture, processing and the scattering of waves by fracture initiating defects (fig. 2).

The intent of this paper is to examine the modes of failure from some of the dominant flaws, to rationalize their relative severity and to quantify their role in structural reliability. Particular emphasis is placed upon the defects created during the fabrication process. The creation of these defects during fabrication is then examined, and links between the important processing variables and structural reliability are established and discussed. The development of associations between failure and processing identifies several major research opportunities.

The characteristics of the general microstructure also influence mechanical properties (fig. 2), especially properties such as the fracture toughness and the high temperature cavitation susceptibility. An important example is the nature of the amorphous phase in liquid phase sintered materials, such as silicon nitride.[4] These general microstructural effects are not afforded explicit attention in the present article. Similarly, defects (and microstructural changes) induced by environmental interactions are of considerable importance in certain ceramics;[5] but again, these phenomena are not specifically addressed in this paper.

## 2. FRACTURE INITIATING DEFECTS

Three major failure categories can be distinguished in ceramic materials. At low or intermediate temperature fracture is elastic and generally, the strength is either invariant with temperature or increases with temperature[2] (fig. 3a). Fracture within this temperature range can occur either from flaws that exist prior to stress application[6,7] (materials with a fine scale microcrostructure), from the coalescence of stress induced microcracks or from flaws smaller than the material grain size (materials with a coarse microstructure). Strong effects of grain size on strength obtain in the coarse grained regime[6] (fig. 3b). In contrast, fracture at elevated temperatures is preceded by some non-linear deformation and the fracture strength diminishes with increase in temperature or decreases in strain-rate (fig. 3a). This fracture process involves the formation and coalescence of cavities; a phenomenon associated with either the diffusive transport of matter from the growing cavity or with viscous hole growth within an amorphous second phase. The three failure classes are examined on a separate basis, because different sources of failure prevail in each regime. Then, explicity consideration is afforded the defects that evolve during fabrication, as a basis for the subsequent analysis of defect generation.

### *2.1. Pre-existent Flaws*

Typical pre-existent flaws include surface cracks, large voids (or void clusters), inclusions and (infrequently) large grains. The surface cracks are created during machining or surface finishing. Most other flaws develop during fabrication. Surface crack and large grain induced fracture are primarily a consequence of residual stress; void related failures are generally related to stress inhomogeneity effects; while inclusion initiated failure involves some combination of residual stress and stress concentrating influences

#### *i) Surface Cracks*

Surface cracks form whenever a hard particle plastically penetrates the surface, as inevitably occurs during grinding, polishing or any other surface finishing process. The cracks develop in response to a residual stress that results from the creation of a confined plastic zone[8](fig. 4). These cracks extend upon application of an external stress $\sigma_\infty$ and induce failure.[9] The initial extension of the crack is stable, because of the dominance of the local residual field (fig. 5). Criticality (as manifest in a maximum value of $\sigma_\infty$ ) develops when the remote stress attains a level, $\sigma_f^\infty$ †, given by;[8]

$$\sigma_f^\infty = [3/(64)^{1/3}]\, K_{IC}\, (\pi\alpha/a_0)^{1/2} \qquad (1)$$

---

†The cracks represented by eqn (1) form primarily along the grinding direction and thus dominate the strength when stresses are applied normal to the grinding direction.[11] The strength parallel to the grinding direction has not been considered in such detail. The character of the transverse cracks is a subject for future study.

where $K_{IC}$ is the fracture toughness, $a_0$ is the initial flaw size and $\alpha$ is a geometric parameter ($\approx 5.8/\pi^2$). This failure process generally has no direct association with processing, except through the influence of microstructure on $K_{IC}$[10] (an issue that will not be examined in the present paper). The distribution of failure strengths is primarily related to the spectrum of machining forces, which dictate the range of flaw radii, $a_0$, generated in the surface. However, it is noted that there should be a tendency for large grained regions to be more frequent sources of failure than would be anticipated from their density on the stressed surface. This expectation is based on the notion that the effective toughness at a large grained zone is smaller than the macro-toughness, whenever the crack area samples a relatively small number of grains. The crack extension at such locations (during grinding), should thus exceed that elsewhere along the surface, at the same level of grinding force. The spatial spectrum of grinding forces vis-a-vis the probability of occurrence of large grained zones would thus dictate the incidence of premature failure from such regions. This is a topic that requires further study.

### *ii.* *Voids*

Large voids and void clusters constitute a frequent failure origin in sintered materials[12,13,14] (fig. 6a). Voids are indirect sources of fracture (because a void does not usually induce a sufficient stress intensification to permit the direct induction of fracture from the void surface). Fracture from voids is typically dictated by the presence of other defects located in their immediate vicinity.[13,15] The defects interact with the stress concentration around the void to produce the fracture (fig. 6b). The nature of these defects is not well comprehended at this juncture. Several possibilities exist. Voids located near the surface can interact with surface cracks.[12] Microcracking could be enhanced in the regions of stress concentration around the void in the presence of an appreciable localized residual stress (e.g. as induced by thermal contraction anisotropy, section 2.3). The material around the void could be mechanically or chemically degraded as manifest in low levels of local toughness.

Several modes of void induced failure exist, although none are of sufficient generality to embrace all observed fracture characteristics. Nevertheless, it is apparent that, because of the statistical nature of the defects that must interact with the voids to produce failure, considerable variability in fracture stress exists even for voids of uniform size[1,13]. Also, the strength is often weakly dependent on void size (fig. 6b). This behavior contrasts with the limited fracture variability encountered with surface cracks of a specified size (eqn. 1)[9]. Voids are thus particularly deleterious with regard to the predictability of failure, based upon nondestructive measurements.[16] An appreciable density of large voids also imposes stringent limitations on the strength enhancement, because reductions in void size have a minimal influence on strength. The only effective means of strengthening is the achievement of a substantial reduction in void density.

A special case of void related failure is associated with the existence of circumferential cavities (fig. 7). These cavities initiate mechanical failure in accord with mechanisms similar to those advanced for void induced failure.

### *iii. Inclusions*

Inclusions are a major source of premature failure. Inclusion induced fracture exhibits a spectrum of possibilities[1], as illustrated in figs. 1 and 8. Failure from each inclusion/host combination should be examined on a separate basis. The first distinguishing feature is the tendency for residual stress associated cracking attributed to thermal contraction mismatch (fig. 8). If the thermal expansion coefficient of the inclusion is appreciably lower than that for the matrix, tensile stresses create radial matrix cracks when the defect exceeds a critical size.[17] This situation can produce severe strength degradation; but such behavior is unusual for structural materials (which must have an intrinsically low thermal expansion coefficient in order to resist thermal shock). Alternately, if the expansion coefficient of the inclusion exceeds that for the matrix, several possibilities can result. Highly contracting, high modulus inclusions will tend to detach from the matrix, and produce a defect comparable in character to a void. Inclusions that are more compliant, or exhibit smaller relative contractions, remain attached to the matrix. The expected failure mode depends upon the elastic modulus and fracture toughness of the inclusion, vis-a-vis the matrix. For example, when the inclusion has a larger toughness than the matrix, stress concentration effects cause fracture to initiate within the matrix, usually from microflaws located within (or adjacent to) the interface. If the bulk modulus of the inclusion also exceeds that of the matrix, the tensile stresses (in a direction suitable for continued extension of the crack due to the applied stress) are confined to a relatively small zone near the poles of the inclusion (fig. 8). For this case, the fracture probability is anticipated to be relatively small, as exemplified by WC inclusions in silicon nitride (fig. 1). Alternatively, when the modulus of the inclusion is small, the maximum tensile stress concentrations occur in the matrix near the equatorial plane. Fracture initiates within this region of the matrix, irrespective of the inclusion toughness. The fracture condition is thus comparable to that for a void. This case is expected to be an important one, because inclusions are often porous (following high temperature mass transport driven by thermal contraction anistoropy) and hence, of low effective modulus. Finally, low toughness (e.g. large grained) inclusions with a similar modulus to the matrix can form sub-critical cracks. The cracks then dictate strength in accord with standard principles of fracture mechanics (e.g. Si inclusions in $Si_3N_4$).

Several modes of fracture that accord with the general principles outlined above have been developed.[1] However, model development is at an elementary stage, and expressions relating fracture to inclusion size and composition have not been adequately correlated. Again, appreciable statistical variability poses concern with regard to fracture prediction based upon non-destructive measurements, and adequate control of defect density is needed to attain acceptable strength levels.

Inclusions usually originate either in the powder source, the powder treatment process or in the green compaction stages of fabrication.† Their elimination as prime sources of premature failure thus resides in the adoption of clean room procedures, proper choices of milling media and in the selection and control of the powder source. These requirements are relatively well comprehended, although not widely utilized.

---

†For example, in $Si_3N_4$, inclusions of WC originate from the milling procedure (which utilizes WC spheres) and inclusions of Si originate in the powder, which may be incompletely nitrided. (LASER processing might reduce Si inclusions?)

Infrequently, inclusions can form during sintering. This would occur if, for example, an extraneous constituent melts and forms a liquid that does not wet the solid phase. The liquid then agglomerates to form an inclusion of appreciable size. Again, adequate control of the powder chemistry provides a solution to the problem.

### *iv. Relative Role of Dominant Flaws*

Most brittle materials can be expected to contain at least two populations of flaws: surface cracks and fabrication defects (fig. 9a). The different spatial character of these two flaw populations signifies a variable relative role of each population in the fracture response observed with different components or test configurations. Strength tests are frequently conducted in flexure; a test procedure which imposes the largest tensile stresses on the specimen surface. Hence, fractures that occur in flexure tests generally originate from surface cracks and flexural strengths often reflect the surface crack population (fig. 9b). Conversely, tensile tests frequently induce failure from fabrication defects and hence, tensile strengths relate primarily to the presence of inclusions, voids, or large grains.

The different spatial character of the important flaw populations also impacts the failure modes experienced by components. For example, thermal stresses usually exhibit a sharp maximum at the surface and hence, thermal shock failures are most sensitive to the surface crack population. In other situations (e.g. rotational stresses in turbine discs) the fabrication flaws are more critical.

## *2.2 Microcrack Coalescence*

Grain boundary located microcracks develop in certain ceramics. The cracks usually occur as a consequence of thermal expansion anisotropy, which leads to the development of large localized stresses[18] (fig. 10a). Calculations of the stresses induced at grain boundaries indicate a logarithmic singularity[19] (fig. 10b), which is not strong enough to induce failure in the absence of pre-existent defects at the triple junction. It has thus been surmized that the cavities which exist at certain junctions are of sufficient size that microcrack initiation can occur at these locations. This premise provides a good estimate of the microcracking condition, but has yet to be afforded a direct experimental validation. The basis for the analysis is the stress intensity factor, K (as deduced from the residual stress) and its variation with crack length (fig. 10c). A peak value of K is found to exist. This peak value is equated to the local fracture resistance in order to deduce a critical microfracture condition. The critical condition can be expressed in terms of a critical grain facet length, $\ell_c$ given by;[20]

$$\ell_c = \frac{2(1+\nu^2)\gamma_{g.b.}}{E(\Delta\alpha\Delta T)^2} \quad \exp\left[-\frac{8\sigma_\infty(1-\nu^2)}{5E\Delta\alpha\Delta T}\right] \qquad (3)$$

where $\gamma_{g.b.}$ is the grain boundary fracture energy, $E$ is Young's modulus, $\Delta\alpha$ is the thermal anisotropy, $\Delta T$ is the cooling range and $\nu$ is Poisson's ratio.

Initial microcrack formation does not usually coincide with failure. Several contiguous microcracks generally need to accumulate (fig. 3b) before a crack of critical size is generated. This process is understood at the conceptual level, but adequate mathematical models have yet to emerge. Failure models in the absence of microcrack interaction[21] provide useful insights, but interaction is likely to be important and an effective solution to the problem requires numerical techniques. Some preliminary studies that include interaction effects have been conducted.[22] However, general relations that describe fracture and reliability within this regime have not yet been developed.

The strong influence of grain size upon the microcracking process suggests that zones of exceptional grain size could be a source of premature failure, particularly if there exists a sufficient number of contiguous grains to provide a coalesced crack of critical size. This has not yet been a widely observed source of brittle fracture. Nevertheless, large grained regions should be regarded as a potential detriment to mechanical performance. Their avoidance through processing control is thus desirable.

### 2.3 *Cavitation Induced Failure*

At elevated temperatures, fracture from pre-existant flaws is frequently suppressed, as demonstrated by the observed stable opening of surface cracks. Critical fractures initiate from other, preferred sites: by means of a process involving the nucleation, growth and coalescence of cavities (fig. 3a).[23] The cavity growth is dictated by diffusion and/or by viscous deformation. The latter process participates in the failure of materials containing amorphous grain boundary phases.[4] The specific origins of failure in such materials have not yet been explicitly determined; although, regions with either an excess thickness of amorphous phase or with a local deviation in chemical compostion (i.e. a low local viscosity) are evident sources of premature failure.

A superior (but still incomplete) comprehension of failure has emerged for predominantly single phase materials. In such materials cavitation typically occurs by a combination of surface and grain boundary diffusion.[24,25,26] Generally, cavities evolve from three grain junctions and extend across the intervening grain facets. The consequences of this cavitation process are illustrated in fig. 11. Occasionally (especially in coarse grained materials) cavities also initiate on two grain junctions.[27] The cavitation is inhomogeneous, and failure evolves from certain preferred microstructural regions. The dominant characteristics of the failure origins are still under investigation.

Recent studies indicate that large grained regions are a strong source of premature failure[22] (fig. 12a), particularly zones containing grains that exceed the average by ∿3. The enhanced failure rate derives from the large stress levels that develop in coarse grained zones by virtue of their high diffusive viscosity (fig. 12b)[†].

Fracture also originates from isolated regions that contain amorphous grain boundary material[27], because of the relative rapidity of the failure process in the presence of viscous hole growth. Inhomogeneous cavitation in the absence of large grained or amorphous zones (figs. 3a, 10) is considered to originate on boundaries with low relative values of the dihedral

---

[†] A high viscosity zone in a viscous solid is analagous to a high modulus inclusion in an elastic solid[21,22]. The stress in this zone can be appreciably larger than the applied stress. The high viscosity of the large grained zone derives directly from the grain size dependence of the creep rate, $\eta \propto d^3$.

angle[†] and/or small values of the surface diffusivity[26] (pertinent to cavities created on the boundary). Low values of these parameters encourage the formation of crack-like cavities (fig. 13) which extend by the transfer of relatively small amounts of matter onto the intervening rain boundaries.

The specific influence of inhomogeneities on creep rupture can be deduced from considerations of diffusive cavity growth (or viscous hole growth) in the presence of viscous constraint from the surrounding material. A typical failure relation is given by;[26,27]

$$t_f \dot{\varepsilon}_\infty \approx 10^2 \left(\frac{D_s \delta_s}{D_b \delta_b}\right)^{1/2} \left(\frac{\gamma_s}{\sigma_\infty d}\right)^{1/2} \left(\sin^{3/2} (\Psi/4)\right) \left(\frac{d}{d_\ell}\right)^2 \qquad (2)$$

where $t_f$ is the failure time, $\dot{\varepsilon}_\infty$ is the steady state creep rate, $\sigma_\infty$ is the applied stress, $d_\ell$ is the local grain size, $d$ is the median grain size, $D_b \delta_b$ is the grain boundary diffusion parameter, $D_s \delta_s$ is the surface diffusion paramter, $\Psi$ is the dihedral angle and $\Omega$ is the atomic volume.

Large grained or amorphous failure zones are clearly influenced by processing, as addressed in the subsequent section. However, regions with low $\Psi$ or $D_s \delta_s$ are not overtly related to processing. Such regions may be an inevitable consequence of grain growth, and the resultant tendency for developing a specific distribution of grain boundary orientations (and a consequent partioning of solutes). Further studies on grain boundary structure and the propensity for creating specific grain boundary orientations are needed in order to examine this issue.

---

[†] presumably a consequence of grain orientations or solutes that yield low values of the surface energy or small surface diffusivities.

### *2.4 Processing Related Defects*

The preceding considerations of failure indicate that several processing sensitive defects exert a major influence on mechanical integrity. Large grained zones are important sources of failure at both low and high temperatures. Large voids and cavities are detrimental to mechanical performance, mostly at low temperatures. Certain inclusions exert a general influence on failure.

Inclusions originate during the powder stage of processing, as outlined in the preceding sections. The formation of large grains, voids and cavities generally relate to events that occur during consolidation. Analysis of the evolution of these defects during sintering constitutes the primary emphasis of the subsequent section.

## 3. DEFECT FORMATION DURING PROCESSING

### *3.1 Large Grains*

Exaggerated grain growth during sintering frequently occurs under conditions that promote the separation of grain boundaries from pores during the final stage.[28,29] This separation event thus constitutes an important phase in the formation of large grain defects, such as those depicted in fig. 12. Consideration of the sequence of events during breakaway[30] indicates that separation can be essentially averted whenever the pore size is maintained below a critical level, $a_c$. The critical size derives from analysis of pore and grain boundary shape changes that occur during the motion of grain boundaries containing pores.

The pore changes reside in the requirement that a continuous gradient of surface curvature be established in order to generate the requisite atom flux from the leading to the trailing surface of the pore (Appendix I, fig. 14). The extent of the shape change depends upon the dihedral angle and upon the normalized pore velocity. Some typical pore shapes for a dihedral angle of $\pi/3$ are shown in fig. 14. The important features to note are that the radius of contact, $a$, remains essentially invariant at low velocities (fig. 14b), while 'steady-state' pore motion prevails; whereas, non steady-state conditions initiate above a critical pore velocity (Appendix I), such that the contact radius diminishes with subsequent increases in net velocity (fig. 14c).

Consideration of pore shape changes with pore velocity does not provide a complete description of the separation event. Grain boundary shapes must also be computed. The specific shapes of migrating grain boundaries depend upon the surrounding grain configurations. An important configuration is depicted in fig. 15a; a configuration in which the disappearance of the small grains constitutes exaggerated grain growth. The ultimate stage of small grain disappearance follows the formation of the three-sided configuration (fig. 15b), whereupon the grain boundary velocity continues to increase as the grain dimension diminishes. The separation of pores located on boundaries between two grains,[†] evidently initiates when the velocity of such pores become smaller than the grain boundary velocity at neighboring grain junctions or grain segments. Pore drag, with a consequent axisymmetric grain boundary distortion, then develops (fig. 16). The characteristic shapes of the distorted grain boundaries can be determined (Appendix I) by requiring that the chemical potential (or driving force) along the grain boundaries be uniform (or slowly

---

[†] Pores at three grain junctions cannot become isolated within grains (in the absence of major instabilities); the pores must, firstly, be displaced from the grain junctions onto two grain interfaces.

varying with position) in order to maintain continuity of motion. The chemical potential is dictated by the two axisymmetric radii of curvature ($R_1$ and $R_2$) illustrated in fig. 16. Then, subject to the boundary condition that the grain boundary inclination at the grain junction be $\pi/3$, the grain boundary shapes depicted in fig. 17 are predicted. Experimental observations of pore drage performed in MgO[31] and $Al_2O_3$[32] (fig. 18) confirm the predicted pore and grain boundary shapes.

Inspection of the grain boundaries subject to pore drag indicates boundary velocity components both parallel and normal to the pore velocity vector (fig. 16). The boundary displacements associated with the normal component cause a net increase in the grain boundary driving force by virtue of the decrease in the curvature $R_2$. The grain boundary configuration is thus basically unstable, and steady-state motion of the complete pore/grain boundary ensemble is impossible. Hence, pore drag will increasingly distort the boundary, and eventually induce separation. The actual separation will occur when the pore velocity attains the level at which the pore contact radius, a , diminishes rapidly with further small increments in pore velocity (thereby, permitting convergence of the boundary onto the pore axis). The grain boundary coalescence is likely to result in a dislocation or sub-grain boundary attached to the pore (especially in the presence of some assymetry), as typically observed[33,34] (fig. 19).

Consequently, stable motion of the pore/grain ensemble and convergence of the pore onto the prospective triple junction can only be assured by averting the onset of the drag. Estimates of breakaway based either on the avoidance of drag or on the requirement that the peak steady state pore velocity be exceeded by the grain boundary velocity suggest (Appendix I) a critical pore size at separation given by[†];

$$a_c^2 = \lambda(\Psi) \left(\frac{D_s \delta_s \Omega}{M_b kT}\right)\left(\frac{\gamma_s}{\gamma_b}\right) \tag{4}$$

where $M_b$ is the grain boundary mobility and $\lambda(\Psi)$ is a coefficient $(1 < \lambda < 10)$ that depends upon both the dihedral angle and the specific separation criterion.

The separation conditon given by eqn (4) is subject to the requirement that the pores have previously been detached from three grain junctions onto two grain junctions.[30] This condition requires that the pore dimension be less than some fraction f of the grain facet length, where $f \sim 1/4$ for a typical dihedral angle ($\Psi \sim 120°$). The resultant pore separation region thus has the form depicted in fig. 20. This separation diagram is similar to that predicted by the phenomenological models.[28,29] The principal differences reside in the numerical coefficients, in the role of the dihedral angle and in explicit grain size effects; (albeit that these differences are likely to be secondary to the common influence of the surface diffusivity and grain boundary mobility). The differences derive from the direct incorporation of unique grain-size-dependent variables into the phenomenological analysis: notably, a grain size dependent driving force and pore spacing. The present, more detailed, conderations of breakaway indicate that such variables are not explicitly involved in the separation process. However, the grain size and grain size distribution have an indirect involvement in breakaway; an involvement related to the placement of grain/pore size trajectories onto the breakaway diagram.

---

[†] Eqn (4) presumes that $M_b$ is driving force independent. The incorporation of variable grain boundary mobilities requires further study.

Determination of grain/pore size trajectories requires consideration of particle rearrangement, pore shrinkage and coalescence and grain growth. During the initial stage, rearrangement occurs, and the size of the average pore may decrease. Thereafter, the pore size increases in approximate proportion with the grain size,[35] because of pore coalescence and concomittant pore shrinkage. Finally, as final density is approached, pore shrinkage dominates and the average pore size is expected to decrease.[36,37] The resultant trajectory is depicted in fig. 20. The extent of the grain and pore growth is dictated primarily by the grain size distribution, the grain boundary mobility, the surface diffusivity and the grain boundary diffusivity.[36,37] Of particular note is the existence of a peak pore size, $\hat{a}$ (fig. 20). Evidently, breakaway can be averted whenever the peak pore size is less than the critical size, $a_c$ . Maintaining $\hat{a}$ below $a_c$ is encouraged by small values of both the grain boundary mobility and the ratio of the grain boundary to the surface diffusivity[37], as well as a narrow particle size distribution.

It may be surmised at this juncture that failure from large grained zones can be averted by devoting attention during processing to local distributions of both solutes (which influence the grain boundary mobility[38] and the surface diffusivity) and powder particle sizes (which determine the grain coarsening tendencies and the adjacence to the critical pore size). Further studies of coarsening and of solute effects are clearly merited, in order to establish the limits on local variability that can be tolerated without encountering exaggerated grain growth.

### 3.2 *Cavity Formation*

Crack-like cavities or 'shrinkage cracks' form as a consequence of inhomogeneity in the green compact. Specifically, regions containing fine particles are subject to rapid densification. The differential in densification induces stresses within the surrounding compact (stresses which can lead to the development of residual cavities). In particular, appreciable stresses evolve as the fine grained zones approach full density. Cavity formation can be analyzed by considering the sequence of events that occur with this phase of the sintering cycle.[39]

The region subject to rapid densification experiences hydrostatic tension (Appendix II), while the surrounding compact develops shear stresses (radial tension and tangential compression), as depicted in fig. 21. Analysis indicates that the radial tension in the compact immediately outside the rapidly shrinking zone invariably exceeds the sintering stress (Appendix II). The pores in this location are thus incapable of shrinkage while the inner zone is densifying. More importantly, for a particle size difference $\gtrsim 1.3$, the radial tension becomes sufficiently in excess of the sintering stress that cavity growth is inevitable. A circumferential cavity then results. The extent of the cavity growth can be ascertained from the strain energy release rate vis-a-vis the lower bound value for creep crack growth, $\mathcal{G}_{cg}$ , giving;[38]

$$\hat{c}/R = \sin^{-1}\left[1 + \sqrt{1 - \frac{\mathcal{G}_{cg}}{2.2\eta R\dot{V}^2}}\right] \qquad (5)$$

where $\hat{c}$ is the cavity length, $\eta$ is the viscosity of the matrix, $R$ is the zone radius and $\dot{V}$ is the differential in the unconstrained shrinkage rate.

Shrinkage of the outer zone subsequent to cavity formation tends to cause cavity closure. Full densification of the outer zone should permit full closure and elimination of the cavity, provided that the initial (compact) densities were similar within the inner and outer zones. However, appreciable differences in initial density or incomplete densification of the outer zone would generally leave a residual void space (fig. 7).

### 3.3 *Large Voids*

The origins of large voids are not well defined at this juncture. Nevertheless, a set of plausible void evolution processes can be established. The range of possibilities emerges by considering the changes in void space that occur during sintering. In the absence of constraint or coarsening (by surface diffusion), individual void spaces must diminish in proportion with the net shrinkage of the body.[†] However, void space modifications can be conjectured in the presence of either constraints (internal or external) or of rapid coarsening.

External constraints can be eliminated by careful design of the sintering fixtures and will thus be excluded from consideration. Internal stresses can develop during sintering as the result of both particle size distributions and particle rotation. The internal stresses have been conjectured as possible sources of void enlargement. Rapid densification of a zone of fine particles is a prominent example of internal stress (fig. 21, Appendix II). The stresses developed outside the rapidly densifying zone are purely deviatoric (the hydrostatic stress is zero) and hence, void

---

[†] Small pores at three grain junctions coalesce and increase in size in direct proportion with the grain size; but, these pores are too small to be the failure origins of the present analysis.

enlargement cannot occur in this region.[†] However, voids can form at the perimeter of the fine grained zone (as discussed above) and may be of appreciable size if the initial density within this zone is considerably smaller than the density of the surrounding powder.

Particle rotation can also generate internal stresses.[40] The rotational forces can generate hydrostatic tension along the equatorial plane of the void, and are thus capable of inducing a spheroidal enlargement of the void. However, the stresses are very small and significant enlargement is considered unlikely; although additional study of this phenomenon is certainly warranted.

Void coarsening occurs by surface diffusion or by evaporation-condensation in the presence of a size distribution of void space. However, in order to achieve densification, the mass transport that procedes in accord with these mechanisms must be minimal relative to mass transport by boundary or lattice diffusion.[41,42] The low coarsening diffusivities required for sintering in conjunction with the relatively large diffusion distances involved in the coarsening of large voids (several times the particle size), suggest that significant enlargement of the large voids that influence fracture is unlikely.

The most probable sources of large voids include: the intitial void (or filler) space in the green compact, and the decomposition of extraneous particles (with a concomittant generation of gaseous phases). In particular, gas generation within the final stage could lead to appreciable expansion of existent voids (in accord with standard viscoelastic behavior). Further

---

[†] It is emphasized that external constraints have been eliminated from consideration; if such constraints existed void enlargement would occur in the presence of shrinkage inhomogeneity.

studies of gas evolution are of paramount importance with regard to void induced failure.

## 4. CONCLUSIONS

It has been demonstrated that a number of important failure origins in ceramics can be associated with microstructural 'defects' generated during processing. These mechanically defective regions of the microstructure consist of large grained zones, large pores or cavities and large inclusions. Determination of the origin of these defects in the processing cycle and their eventual elimination provides an important processing challenge.

The formation of these processing defects is not well understood, particularly at the quantitative level. Some considerations pertinent to the creation of large grains and large pores have been presented. More detailed analysis of the specific mechanisms of pore/grain boundary breakaway and of void space enlargement are needed before an ability to predict and control defect development can be established. Such studies represent an important research direction for processing science.

## ACKNOWLEDGMENT

This work was supported by the Director, Office of Energy Research, Office of Basic Energy Sciences, Materials Science Division of the U.S. Department of Energy under Contract No. W-7405-ENG-48 and by the U.S. Office of Naval Research, under Contract No. N00014-79-C-0159,

# APPENDIX I

## Pore and Grain Shapes During Sintering

### a) Pore Shapes

The motion of pores attached to grain boundary must result in pore shape changes that provide the gradient in surface curvation needed to create an atom flux from the leading to the trailing surface of the pore (fig.14). By specifying the pore velocity, $v_p$, and requiring that the dihedral angle, $\Psi$ , remain constant, the pore shape can be calculated as a function of pore velocity. Results have been obtained[30] for pore motion by surface diffusion. A linearized, two-dimensional solution is presented here in order to indicate the essential features of the analysis. Detailed results can be found elsewhere[30]

For a pore moving by surface diffusion, the atom flux at a surface element, ds, is given by ;[24]

$$J_s = \pm \frac{D_s \delta_s \gamma_s}{kT} \left(\frac{d\kappa}{ds}\right) \tag{A1}$$

where $D_s \delta_s$ is the surface diffusion parameter, $\gamma_s$ is the surface energy, $\kappa$ is the curvature, and kT has its usual meaning. Defining $\theta$ as the angle between the velocity axis and the surface normal, eqn. (A.1) becomes:

$$J_s = \pm \frac{D_s \delta_s \gamma_s}{kT} \sqrt{1-\cos^2\Theta} \left(\frac{d^2\cos\theta}{dx^2}\right) \tag{A2}$$

where the positive sign refers to the leading surface of the void and the negative sign relates to the trailing surface. Conservation of matter dictates that:

$$\frac{dJ_s}{dx} = \frac{v_p}{\Omega} \tag{A3}$$

Symmetry requires that the net flux across the void axis be zero, and thus,

$$J_s = \frac{v_p}{\Omega} x \tag{A4}$$

Combining (A.2) and (A.4), the differential equation that describes the void shape becomes:

$$\sqrt{1-\cos^2\theta}\left(\frac{d^2\cos\theta}{dx^2}\right) = \pm \frac{V_p kTx}{D_s \delta_s \gamma_s \Omega} \tag{A5}$$

When both the dihedral angle, $\Psi$ , and the velocity are small, the surface tangent does not deviate appreciably from the original grain boundary plane (i.e., $\theta \rightarrow \frac{\pi}{2}$); then $\kappa \cong d^2y/dx^2$; $ds \cong dx$ and $\cos\theta \cong dy/dx$. The differential equation (A.5) then becomes:

$$\frac{d^3y}{dx^3} = \pm \frac{v_p kTx}{D_s \delta_s \gamma_s} = \pm \beta x \tag{A6}$$

This differential equation can be readily solved in closed form, subject to the appropriate boundary conditions. For both surfaces, symmetry requires that $dy/dx = 0$ at $x = 0$. The equilibrium dihedral angle, $\Psi$ , must be retained in the presence of grain boundary or lattice diffusion, hence;

$$\Psi_1 + \Psi_2 = \Psi \tag{A7}$$

where $\Psi_1$ and $\Psi_2$ are the tangents at the leading and trailing edges respectively. The surface curvature $(d^2y/dx^2)$ must be the same for both surfaces at $x = a$. Imposing these boundary conditions, equation (A6) yields the following relations for the pore surfaces:

$$\left(\frac{y_1}{a}\right) = -\left[\left(\frac{x}{a}\right)^2 - 1\right]\frac{\Psi}{4} - \left(\frac{\beta a^3}{24}\right)\left[\left(\frac{x}{a}\right)^4 - 6\left(\frac{x}{a}\right)^2 + 5\right]$$

$$\left(\frac{y_2}{a}\right) = -\left[\left(\frac{x}{a}\right)^2 - 1\right]\frac{\Psi}{4} + \left(\frac{\beta a^3}{24}\right)\left[\left(\frac{x}{a}\right)^4 - 6\left(\frac{x}{a}\right)^2 + 5\right] \tag{A8}$$

A more detailed, finite difference, analysis for an axisymmetric pore[30] indicates similar pore distortions. However, the analysis also reveals that steady state pore motion can only occur up to a peak normalized velocity,

$$V_c(\Psi) \equiv \frac{V_p k T a_o^3}{D_s \delta_s \Omega \gamma_s} \tag{A9}$$

where $V_c$ ranges from 1.5 for a dihedral angle of 160° to 7 for a dihedral angle of 60°. At velocities in excess of $V_c$, non steady-state pore motion initiates and the contact radius $a$ diminishes rapidly with further increases in the net pore velocity.

Another result of interest is the inclination $\phi$ between the grain boundary tangent and the plane of pore contact. This is given for the axisymmetric pore by;

$$\phi \approx 0.05 \frac{V_p k T a_o^3}{D_s \delta_s \gamma_s \Omega} \tag{A10}$$

where $a_o$ is the initial pore contact radius.

b) Grain Boundary Shapes

The grain boundary shape is determined by the driving force (boundary curvatures) and the grain boundary mobility. Preliminary grain boundary shapes are calculated by assuming uniform driving force and mobility conditions. When a pore is attached to a grain boundary and pore drag initiates, an axisymmetric boundary shape develops in the vicinity of the pore (fig. 16). The boundary thus exhibits two curvatures, $\kappa_1$, and $\kappa_2$ (fig. 16) that determine the driving force. The axisymmetric curvature $\kappa_2$ permits the existence of a net positive driving force in the direction of pore motion, even when the in-plane curvature $\kappa_1$ is negative (a curvature normally indicative of boundary motion in the opposite direction).

The driving force, attributed to the grain boundary curvature, on the boundary containing the pore, is given by,[30]

$$F = \gamma_b \left[ \frac{d^2y}{dx^2} \left[1 + (dy/dx)^2\right]^{-3/2} + \frac{1}{y}\left[1 + (dy/dx)^2\right]^{-1/2} \right] \tag{A11}$$

while the driving force on the other two boundaries is

$$F = 2\gamma_b/R \tag{A12}$$

where R is their radius of curvature. Equating these driving forces in accord with our uniformity assumption, we obtain

$$\frac{dp}{dx} = -\frac{2}{R}\left(1 + p^2\right)^{3/2} + \frac{1}{y}\left(1 + p^2\right) \tag{A13}$$

where $p = dy/dx$. This equation can be solved, using a finite difference procedure, subject to the boundary condition that the dihedral angle at the three grain junction be $2\pi/3$. The results are described in the text (fig. 17).

### c) Estimates of Pore Separation

Pore separation can be considered to occur as an inevitable consequence either of the initiation of pore drag or of a grain boundary velocity that exceeds the peak steady-state pore velocity. Estimates of separation obtained for both criteria yield similar results.

The pore drag initiation criterion requires that the steady-state motion of pores with grain boundaries be established, then, the pore velocity is allowed to become incrementally smaller than the boundary velocity. Steady-state boundary motion pertains on boundaries with an essentially spherical surface, radius R. Attachment of a pore to such a boundary requires that the grain boundary tangent, $\phi$ , satisfy a geometric requirement, dependent upon the void radius (a), given by;

$$\phi \approx dy/dx|_{x=a} = a\Big/\sqrt{R^2-a^2} \qquad \text{(A14)}$$

However, $\phi$ dictates the pore velocity (eqn A10), while R establishes the boundary velocity according to;

$$v_b = 2\gamma_b M_b/R \qquad \text{(A15)}$$

By requiring $v_p$ to be incrementally smaller than $v_b$ , the condition for initiating instability can be derived from eqns (A10), (A14) and (A15) as

$$(a_o/R)^2 < 1 - \left(\frac{10\Omega D_s \delta_s \gamma_s}{kTa_o^2 M_b \gamma_b}\right)^2 \qquad \text{(A16)}$$

Hence, an instability is most likely to initiate when $R$ is at its <u>largest</u> value: because $\phi$ decreases as $R$ increases. The maximum value of $R$ during exaggerated grain growth (fig. 15a) pertains when the boundary is of uniform width. At this stage, $R = d_s$ (where $d_s$ is the size of the small grains). The separation condition thus becomes,

$$a_o^2 > \frac{10(\Omega D_s \delta_s \gamma_s / kTM_b \gamma_b)}{\sqrt{1 - (a_o/d_s)^2}} \tag{A17}$$

Since it is geometrically required that $d_s > 2a_o$ (see section 3.1), eqn (A17) reduces to the result given by eqn (4) in the text.

Alternately, separation can be considered to initiate when the grain boundary velocity (eqn A15) exceeds the peak steady state pore velocity (eqn A9);

$$a_o^2 \geqslant \left(\frac{R}{a_o}\right)\left(\frac{V_c(\Psi)}{2}\right)\left(\frac{\Omega D_s \delta_s \gamma_s}{kTM_b \gamma_b}\right) \tag{A18}$$

where $R$ is now the curvature of the grain boundary remote from the pore (where it is undistorted by pore drag). Hence, the most stringent condition for the avoidance of breakaway, in accord with this criterion, occurs when $R$ is at its <u>smallest</u> value. The grain breakaway radius of curvature is at its smallest in the three-sided grain configuration that precedes grain disappearance (fig. 15b). For this grain configuration separation is averted if the pore converges onto the prospective three grain junction, $R \sim \sqrt{3}a$, before eqn (A18) can be satisfied. The critical separation condition thus becomes

$$a_o^2 \geqslant [\sqrt{3}\, V_c(\Psi)/2]\, (\Omega D_s \delta_s \gamma_s / kTM_b \gamma_b) \tag{A19}$$

Subsequent, less stringent, separation events would be characterized either by eqn (A18) or by eqn (A17), depending upon the grain size and grain configuration.

## ACKNOWLEDGMENT

The author wishes to express appreciation for financial support of the work described in this paper by both the Director, Office of Energy Research, Office of Basic Energy Sciences, Materials Science Division of the U.S. Department of Energy under Contract No. W-7405-ENG-48 and by the Office of Naval Research under Contract No.N-00014-79-C-0159. The opinions expressed in this paper are personal, but emerged from extensive discussion with many of my colleagues. In particular, I wish to express my gratitude to the following colleagues for their stimulating conversation: R. M. Cannon, R. L. Coble, A. H. Heuer, S. M. Wiederhorn, D. R. Clarke, R. W. Rice, A. Glaeser and L. De Jonghe.

## APPENDIX II

### Inhomogeneity Stresses During Sintering

Zones consisting of fine particles shrink during sintering at a more rapid rate than the surrounding, comparatively coarse-grained matrix (fig. 21). Stresses must develop as a consequence of this shrinkage inhomogeneity. The stress evolution can be analyzed by establishing an analogy with the transformation of a particle contained in a linearly viscous matrix.

The pore volume V in a zone containing particles of size b diminishes at a rate given by;[26]

$$\dot{V} = \frac{9\Omega D_b \delta_b}{\pi k T b^3 (1-f)^3} \left[\sigma_\ell - (1-f)\sigma_\infty\right] \tag{A20}$$

where f is the fraction of the grain facet occupied by the pore, $\sigma_\ell$ is the local stress that develops because of inhomogeneity, b is the grain facet length and $\sigma_0$ is the sintering stress ($\sigma_0 \sim 2\gamma_s \sin(\Psi/2 - \pi/6) / \sqrt{3} fb$). The unconstrained difference in volumetric strain-rate that exists between a zone of small particles, $b^i$, and a larger grained matrix, $b^o$, is thus;[39]

$$\Delta\dot{e}^T = (9/\pi)(\Omega D_b \delta_b / kT)\left[\frac{\sigma_\ell - (1-f^i)\sigma_0^i}{(1-f^i)^3\,(b^i)^3} + \frac{\sigma_0^o}{(1-f^o)^2 (b^o)^3}\right] \tag{A21}$$

where the superscripts i and o refer to the fine and coarse grained zones respectively. This unconstrained strain is analogous to a transformation strain. It can thus be directly related to the stress $\sigma_\ell$ that develops within the fine-grained zone;[39]

$$\sigma_\ell = 4\eta\, \Delta\dot{e}^T \tag{A22}$$

where $\eta$ is the viscosity of the matrix,

$$\eta = \pi k T (b^o)^3 (1-f^o)^3 / 9 D_b \delta_b \Omega \qquad \text{(A23)}$$

Eliminating the transformation strain from eqns. (A19) and (A20) and solving for the shrinkage from eqn. (A18), the local stress becomes,[31]

$$\sigma_\ell \approx \frac{2\gamma_s \sin(\Psi/2 - \pi/6)}{\sqrt{3}\, f^i b^i} (1-f^i) \qquad \text{(A24)}$$

This stress is hydrostatic, regardless of the shape of the fine-grained zone.

The stresses in the coarse-grained zone depend on the shape of the shrinkage inhomogeneity. For an approximately spherical zone;[39]

$$\sigma_r = \sigma_\ell (R/r)^3 \quad : \quad \sigma_\theta = -(\sigma_\ell/2)(R/r)^3 \qquad (r \geqslant R) \qquad \text{(A25)}$$

where $\sigma_r$ and $\sigma_\theta$ are the radial and tangential stresses, respectively, $R$ is the zone radius and $r$ is the distance from the zone center. The stresses are deviatoric ($\sigma_r + 2\sigma_\theta = 0$). The matrix is thus subject to enhanced shear deformation, but neither the macroscopic shrinkage nor void growth behavior are affected by the shrinkage inhomogeneity.

This approach can also be used to predict the particle size ratio that initiates circumferential cavity formation. The essential requirement is;[39]

$$b^o/b^i \geqslant 1.3 \qquad \text{(A26)}$$

## REFERENCES

1. A. G. Evans, M. E. Meyer, K. W. Fertig, B. I. Davis and H. R. Baumgartner, Jnl. of Non-Destructive Evaluation, 1 (1980) 111.
2. R. W. Davidge and A. G. Evans, Mater. Sci. Eng. 6 (1970) 281.
3. B. T. Khuri-Yakub, G. S. Kino and A. G. Evans, Jnl. Amer. Ceram. Soc., 63 (1980) 65.
4. F. F. Lange, B. I. Davis and D. R. Clarke, Jnl. Mater. Sci. 15 (1980) 601.
5. F. F. Lange, B. I. Davis and D. R. Clarke, Jnl. Mater. Sci. 15 (1980) 616.
6. R. W. Rice, Fracture Mechanics of Ceramics, (Ed. R. C. Bradt, D. P. H. Hasselman and F. F. Lange) Plenum, New York (1974) vol. 1, 323.
7. R. W. Rice, Processing of Crystalline Ceramics, (Ed. H. Palmour and R. F. Davis) Plenum, N.Y. (1978) 303.
8. B. R. Lawn, A. G. Evans and D. B. Marshall, Jnl. Amer. Ceram. Soc., 63 (1980) 574.
9. D. B. Marshall, B. R. Lawn, and P. Chantukil, Jnl. Mater. Sci., 14 (1979) 2225.
10. A. G. Evans, A. H. Heuer and D. L. Porter, Fracture 1977 (Ed. D. M. R. Taplin), Univ. Waterloo Press (1977), vol. 1, 301.
11. R. W. Rice and J. J. Mecholsky, The Science of Ceramic Machining and Surface Finishing, NBS Special Publication 562 (1979) 351.
12. R. W. Rice, Treatise on Materials Science and Technology, (Ed. H. Herman) Academic Press, Vol. 11 (1977) 189.
13. A. G. Evans, D. S. Biswas and R. M. Fulrath, Jnl. Amer. Ceram. Soc. 62 (1979) 101.
14. S. G. Seshadri and M. Srinivasan, Jnl. Amer. Ceram. Soc., in press.
15. F. I. Baratta, Jnl. Amer. Ceram. Soc., 61 (1978) 490.

16. J. R. Richardson and A. G. Evans, Jnl. Non-Destructive Evaluation 1 (1980), 37.

17. F. F. Lange, Fracture Mechanics of Ceramics (Ed. R. C. Bradt, F. F. Lange and D. P. H. Hasselman) Plenum, New York (1978) vol. 4, 799.

18. J. A. Kuzyk and R. C. Bradt, Jnl. Amer. Ceram. Soc. 56 (1973) 420.

19. A. G. Evans, Acta Met. 26 (1978) 1845.

20. Y. Fu, M. S. Thesis, U. C. Berkeley (June 1981).

21. F. A. McClintock, Fracture Mechanics of Ceramics, ibid. (1974), vol. 1, 93.

22. R. G. Hoagland and J. D. Embery, Jnl. Amer. Ceram. Soc. 63 (1980) 404.

23. A. G. Evans and A. S. Rana, Acta Met. 28 (1980) 129.

24. T. J. Chuang, K. I. Kagawa, J. R. Rice and L. B. Sills, Acta Met. 27 (1979) 265.

25. J. R. Porter, W. Blumenthal and A. G. Evans, Acta Met., in press.

26. C. H. Hsueh and A. G. Evans, Acta Met., in press.

27. S. M. Johnson, W. Blumenthal and A. G. Evans, to be published.

28. R. J. Brook, Jnl. Amer. Ceram. Soc. 52 (1969) 56.

29. F. Carpay, Ceramic Microstructures (Ed. R. M. Fulrath and J. A. Pask), Westview, Boulder (1976) p. 261.

30. C. H. Hsueh and A. G. Evans, to be published.

31. M. Sakar an, to be published.

32. M. A. Spears, M. S. Thesis, U. C. Berkeley, (Sept. 1981).

33. J. Porter, private communication.

34. D. R. Clarke, private communication.

35. W. D. Kingery and B. Francois, Sintering and Related Phenomena (Ed. G. Kuczynski) Gordon and Breach (1967) p. 471.

36. R. M. Cannon, to be published.

37. M. A. Spears and A. G. Evans, to be published.

38. M. F. Yan, R. M. Cannon and H. K. Bowen, Ceramic Microstructures, ibid., p. 276.

39. A. G. Evans, Jnl. Amer. Ceram. Soc., to be published.

40. G. Petzow and H. E. Exner, Z. Metallkde 67 (1976) 611.

41. R. L. Coble and R. M. Cannon, Processing of Crystalline Ceramics (Ed. H. Palmour and R. F. Davis), Plenum (1978) p. 151.

42. M. F. Ashby, Acta Met. 22 (1974) 275.

43. T. Mori, M. Okaba and T. Mura, Acta Met. 28 (1980) 319.

# FIGURE CAPTIONS

Fig. 1. Effects of defect type on the fracture strength of hot pressed $Si_3N_4$.

Fig. 2. A schematic indicating relations between studies of fracture, processing, and NDE.

Fig. 3. a) A typical effect of temperature on the strength of ceramics, indicating a region of dominance by pre-existent flaws at low temperatures and cavitation induced failure at elevated temperatures.

b) A typical trend in fracture strength with grain size, indicating fracture from pre-existent flaws at small grain sizes and fracture at large grain sizes dictated either by microcrack coalescence or by flaws smaller than the grain size.

Fig. 4. A schematic indicating the formation of surface cracks during machining.

Fig. 5. The stable growth of machining induced cracks during a sterngth test, indicating the stress maximum which coincides with the measured strength.

Fig. 6. a) A large void fracture origin in SiC (courtesy M. Srinivasan) scanning electron micrograph.

b) A schematic indicating a void fracture model and the void size dependence of the strength: m is the shape parameter associated with the size distribution of the circumferential flaws.

Fig. 7. A scanning electron micrograph of a crack-like cavity in SiC (courtesy M. Srinivasan)

Fig. 8. A schematic indicating the various types of inclusion initiated fracture processes.

Fig. 9. a) A schematic indicating the existence of two dominant flaw populations: surface cracks and fabrication defects.

b) The failure incidence from the two populations typically encountered in a flexure test.

Fig. 10. a) A schematic indicating a four grain arrangement and the orientations of maximum and minimum thermal contraction.

b) The residual stresses along the grain boundaries calculated for the four grain configuration.

c) The stress intensity factors for a crack located at the three grain junctions.

Fig. 11. A scanning electron micrograph of cavities in $Al_2O_3$ formed during high temperature mechanical testing.

Fig. 12. a) A scanning electron micrograph of a large grained high temperature fracture origin in $Al_2O_3$.

b) A schematic indicating the relation between the high viscosity and high stress in the large grained zone.

Fig. 13. A schematic indicating the equilibrium and crack-like cavities observed in fine-grained $Al_2O_3$.

Fig. 14. Pore shapes that develop during axial pore motion for pores attached to grain boundaries (a) stationary pore (b) steady state pore motion at the specified normalized velocity (c) non steady state pore motion at high net velocities.

Fig. 15. a) A large grain surrounded by small grains which are eliminated during grain growth.

b) A three-sided grain typical of grain morphologies before final disappearance.

Fig. 16. The axisymmetric configuration that develops during pore drag.

Fig. 17. Calculated shapes of grain boundaries in the axisymmetric configuration.

Fig. 18. Scanning electron micrograph of a pore attached to a migrating grain boundary in MgO.

Fig. 19. Transmission electron micrographs of (a) dislocations attached to intergranular pores (courtesy J. Porter), (b) a sub-grain attached to an intergranular pore (courtesy D. R. Clarke).

Fig. 20. A final stage sintering map indicating the separation region and an expected grain/pore coarsening trajectory.

Fig. 21. A schematic indicating the stresses that develop following the rapid shrinkage of a zone of fine-grained particles in a coarse-grained matrix.

The dependence of the fracture strength of silicon nitride on the inclusion size.

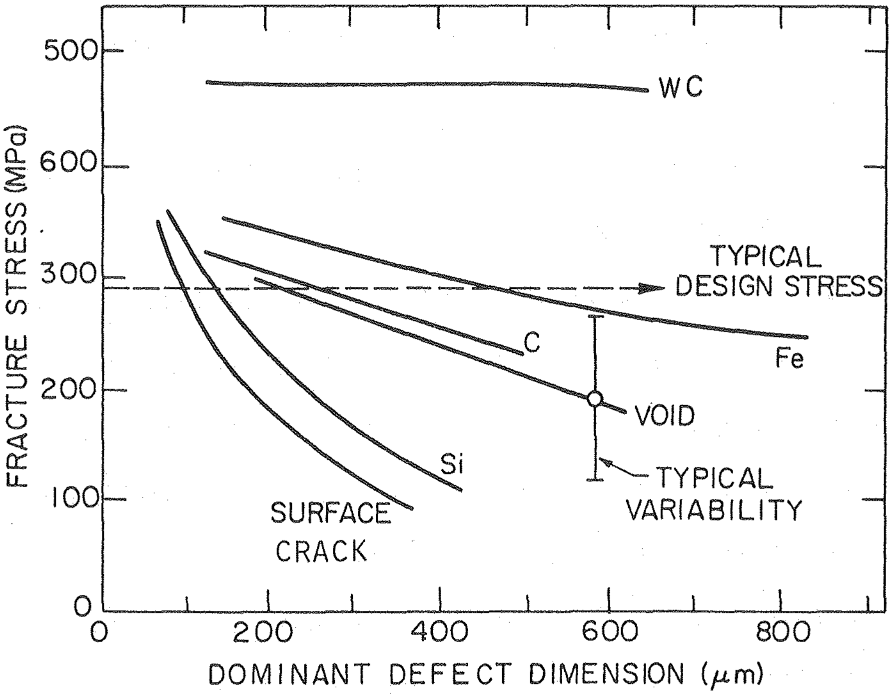

XBL 797-10504

Fig. 1

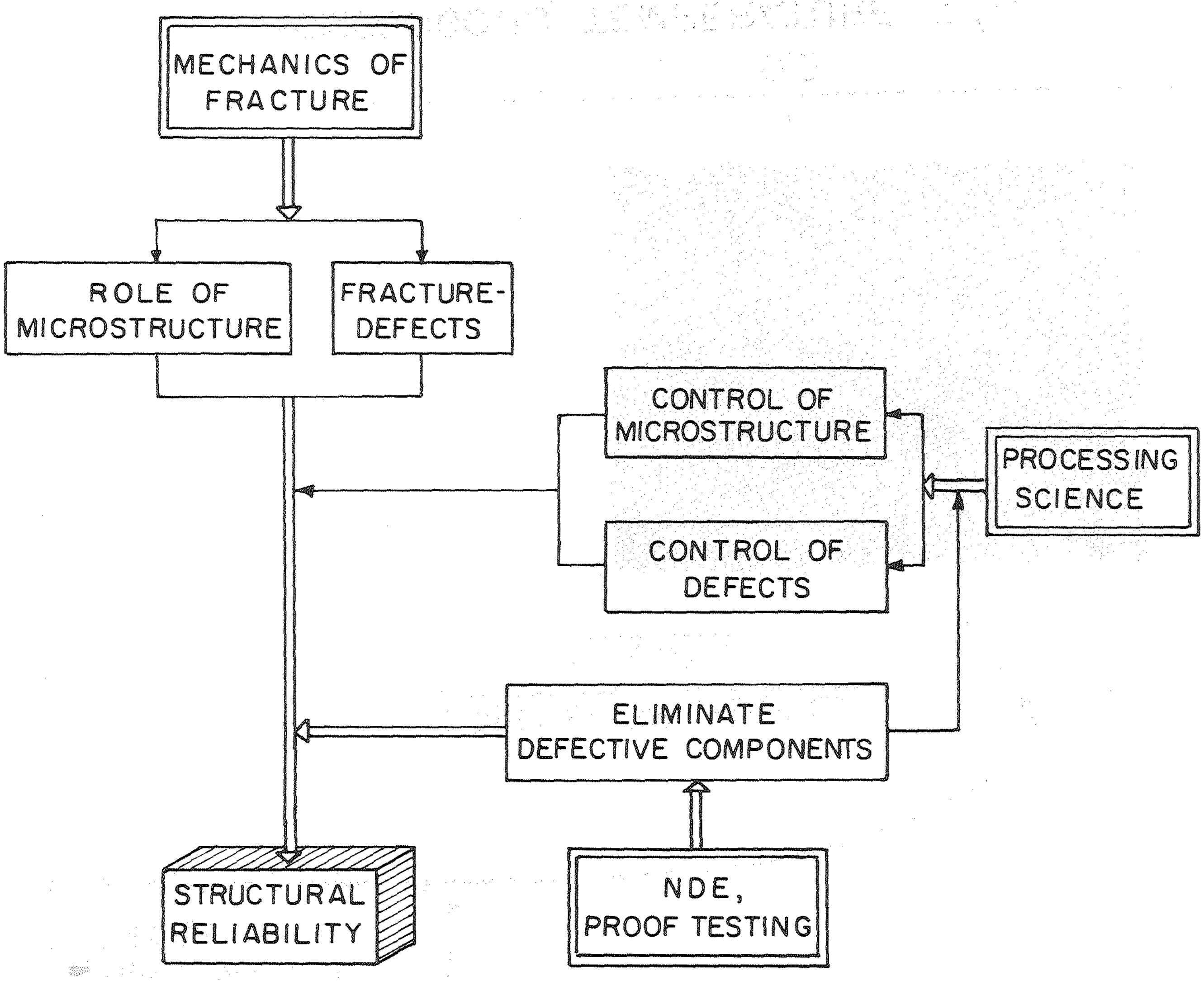

XBL813-5424

Fig. 2

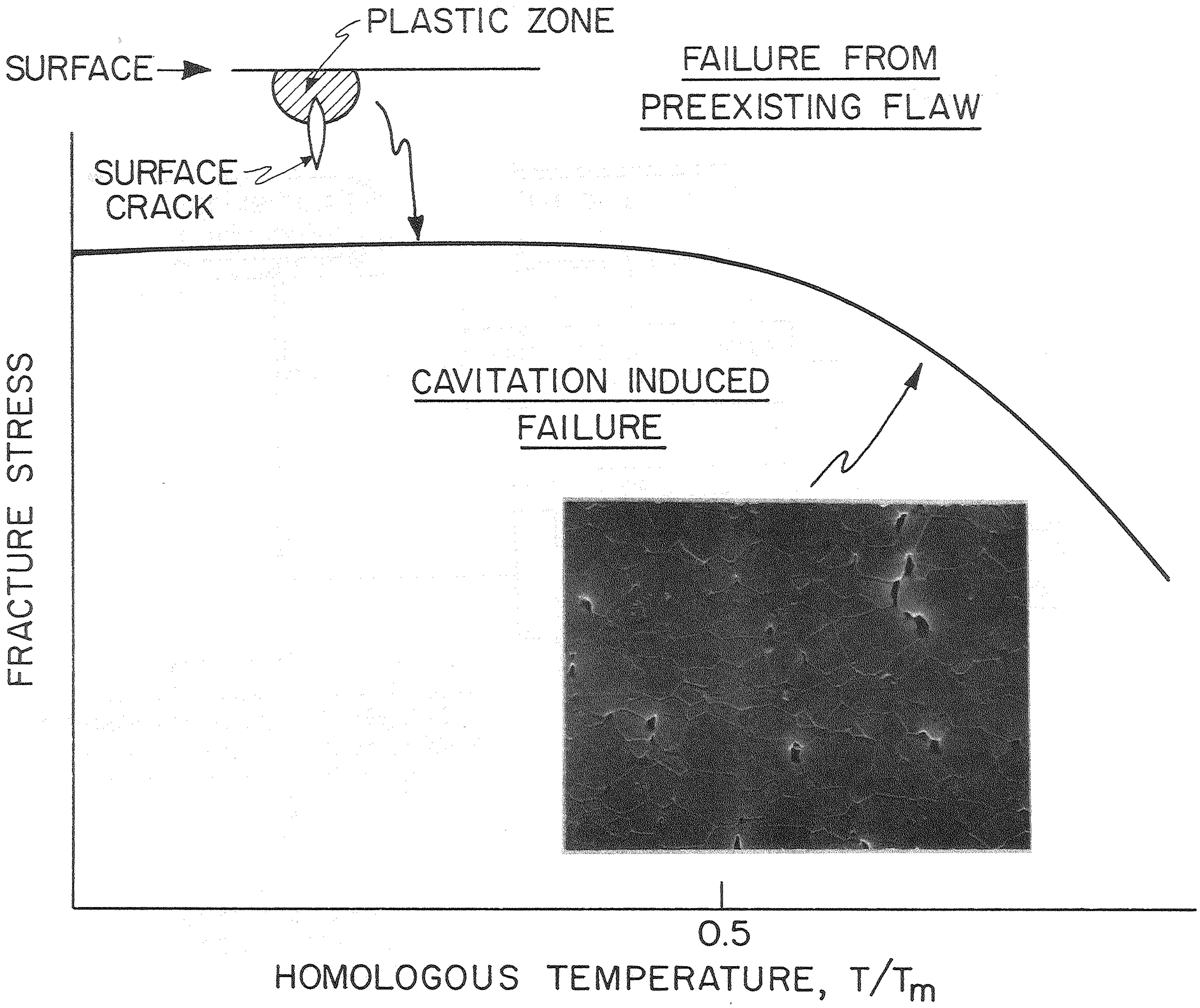

Fig. 3a

XBB 813-2479

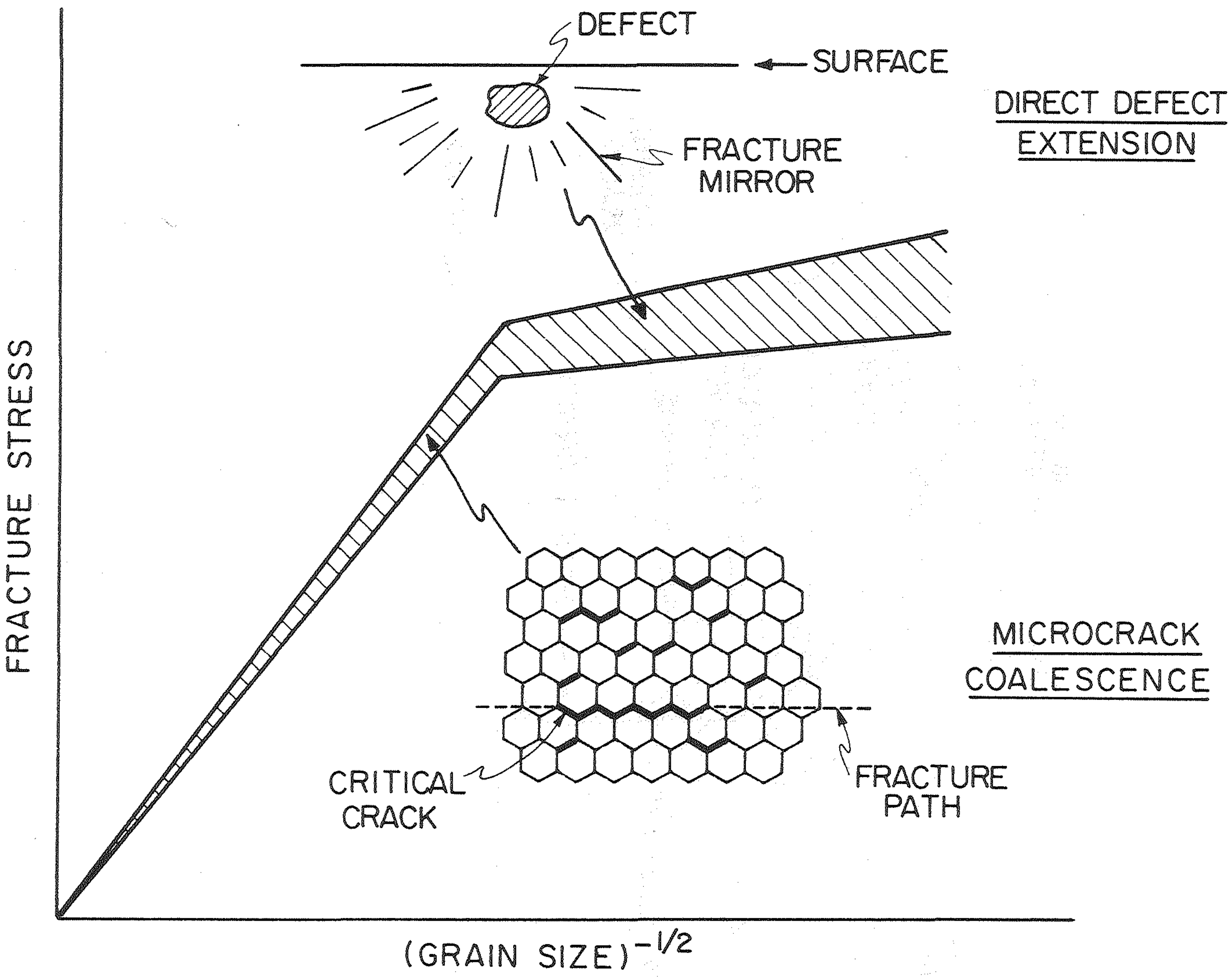

XBL 811-5031

Fig. 3b

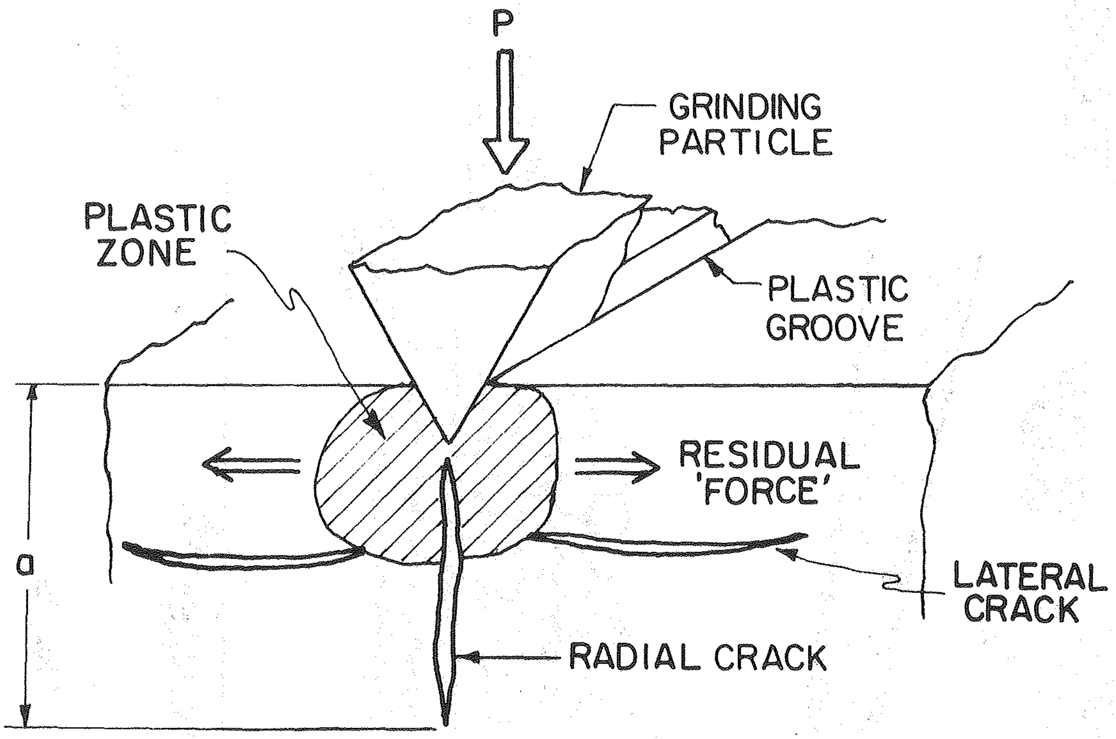

XBL 811-5022

Fig. 4

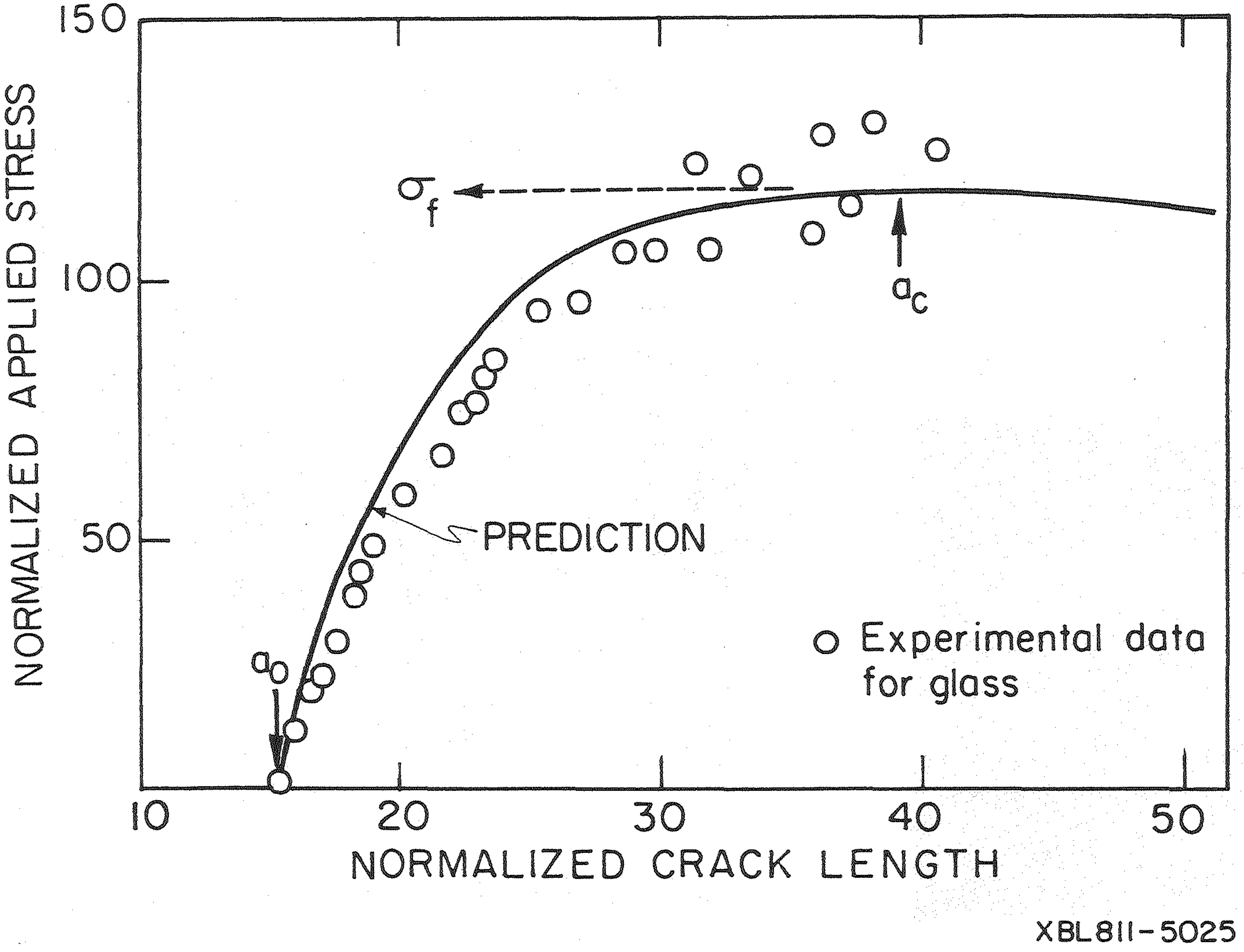
150
100
50
10
20
30
40
50
NORMALIZED APPLIED STRESS
NORMALIZED CRACK LENGTH
$\sigma_f$
$a_c$
$a_o$
PREDICTION
○ Experimental data for glass
XBL811-5025

Fig. 5

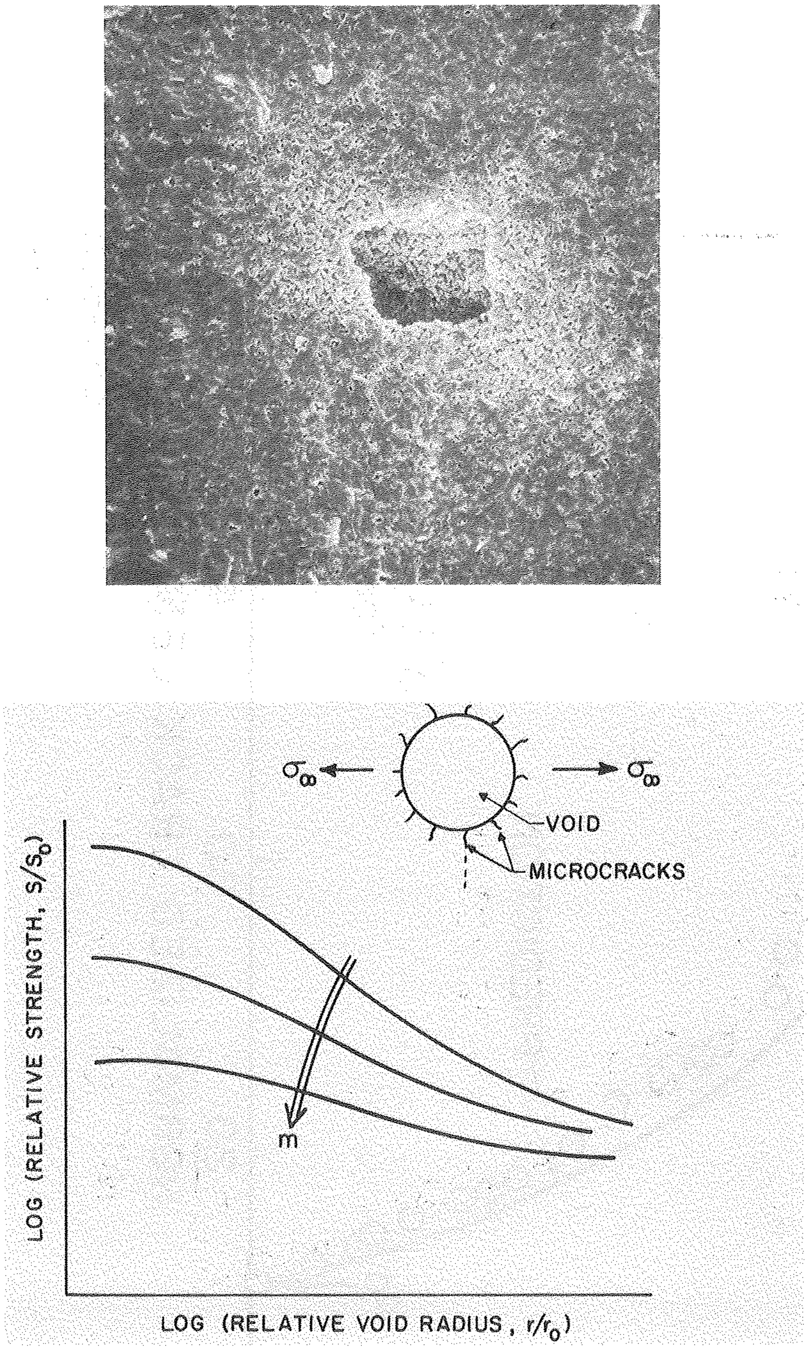

XBB814-3792

Fig. 6

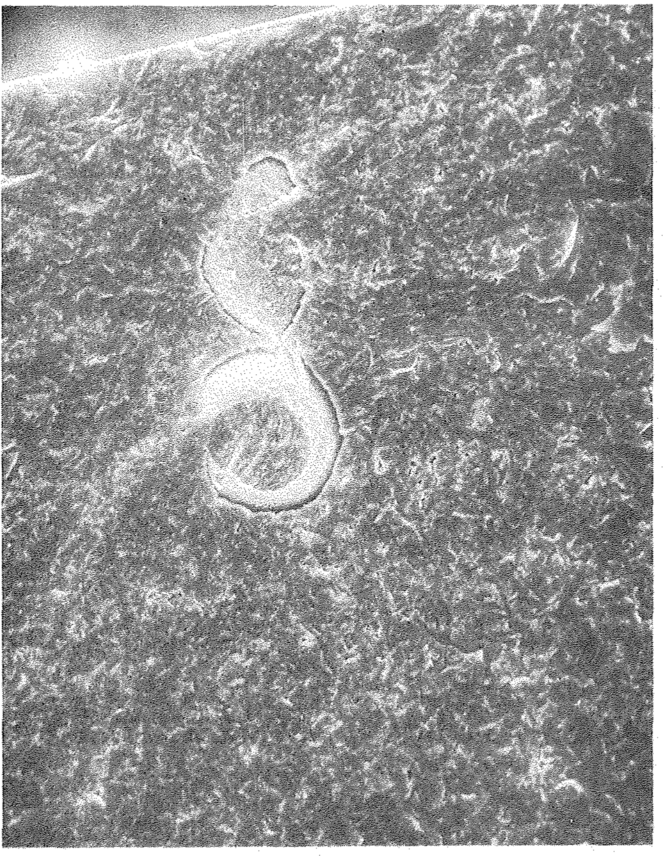

XBB814-3230A

Fig. 7

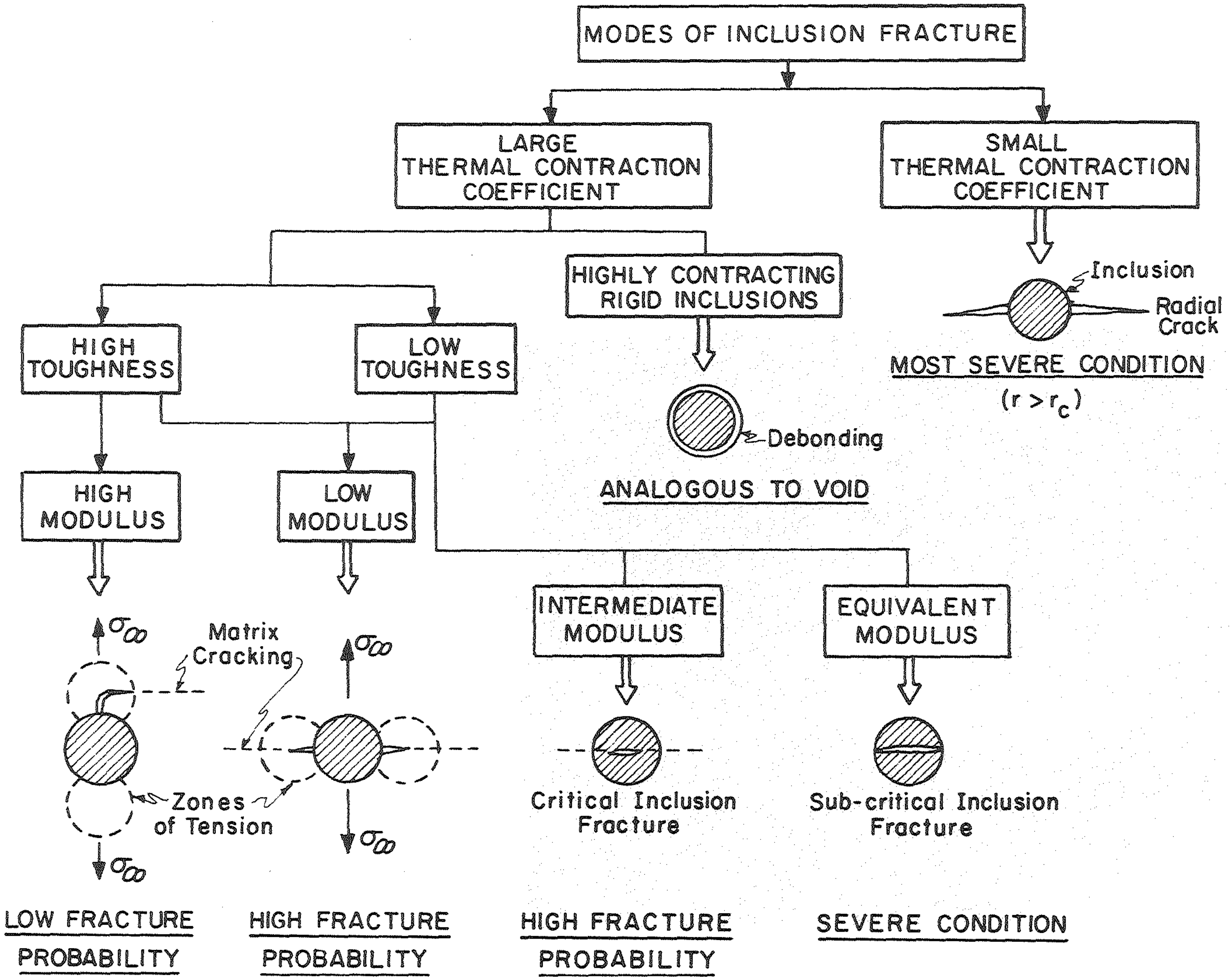

XBL 811-5024

Fig. 8

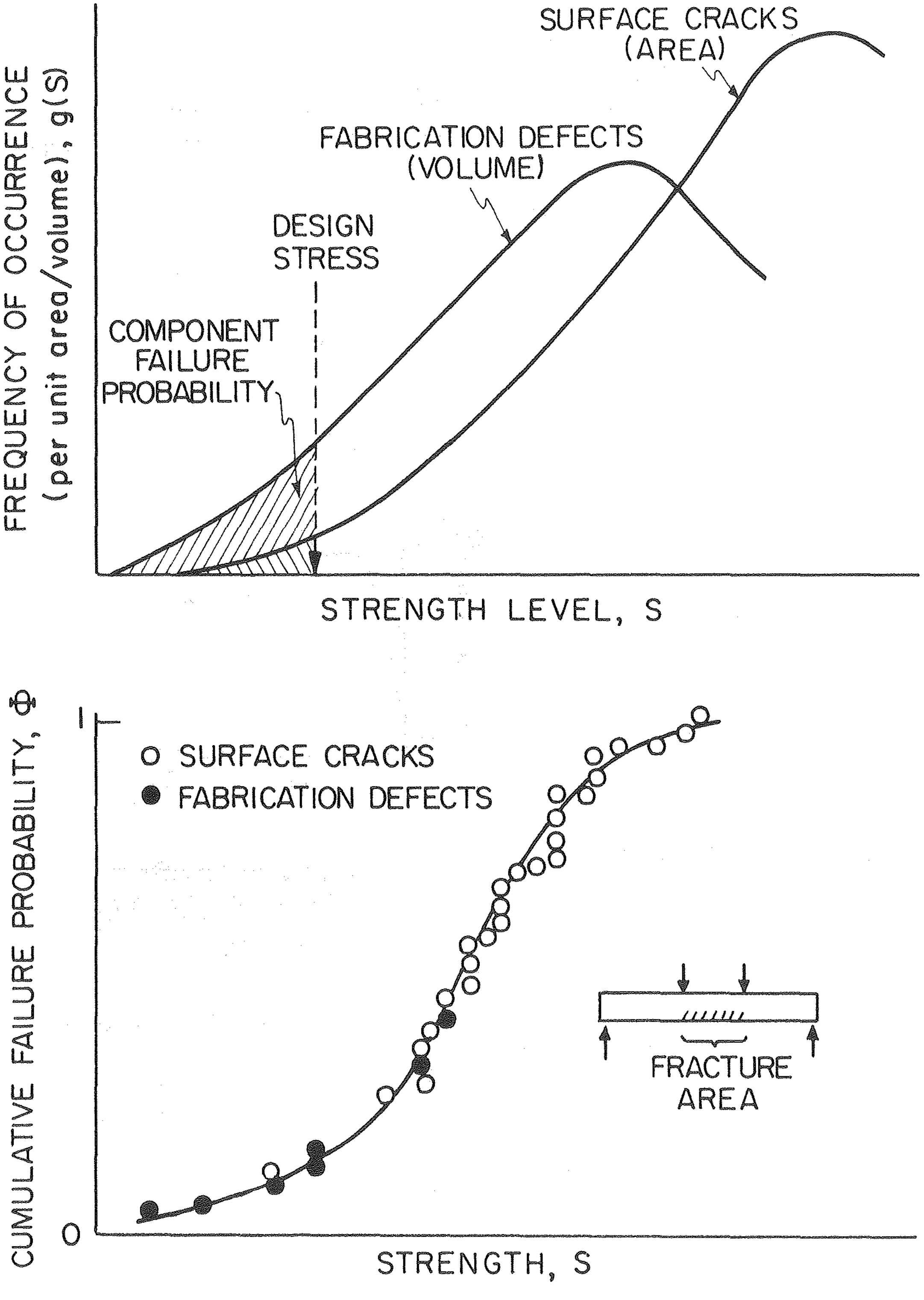

XBL 811-5028

Fig. 9

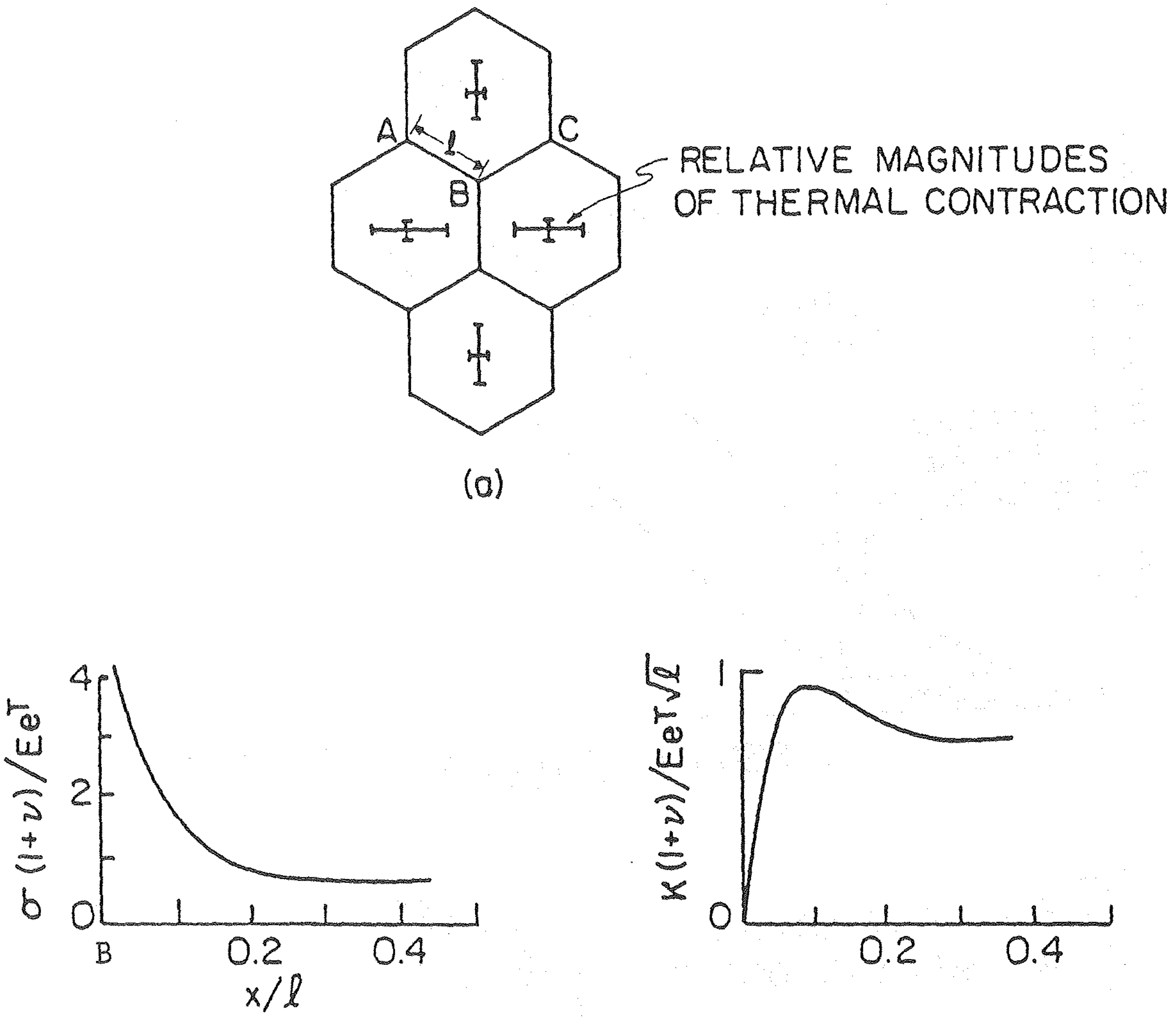

(a)

(b) STRESS ALONG FACET

(c) STRESS INTENSITY FOR DEFECT LOCATED AT B

XBL811-5033

Fig. 10

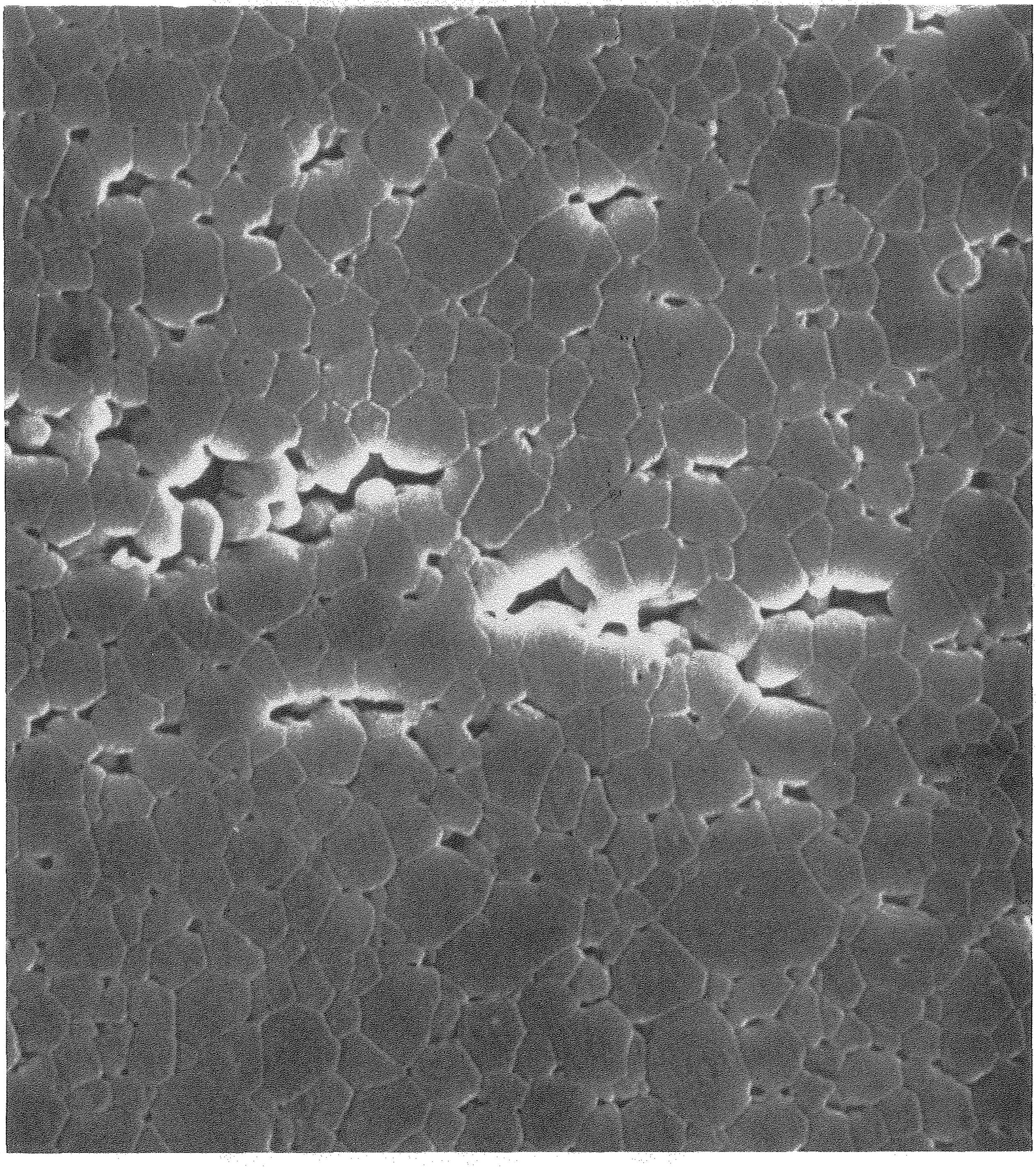

XBB814-3790

Fig. 11

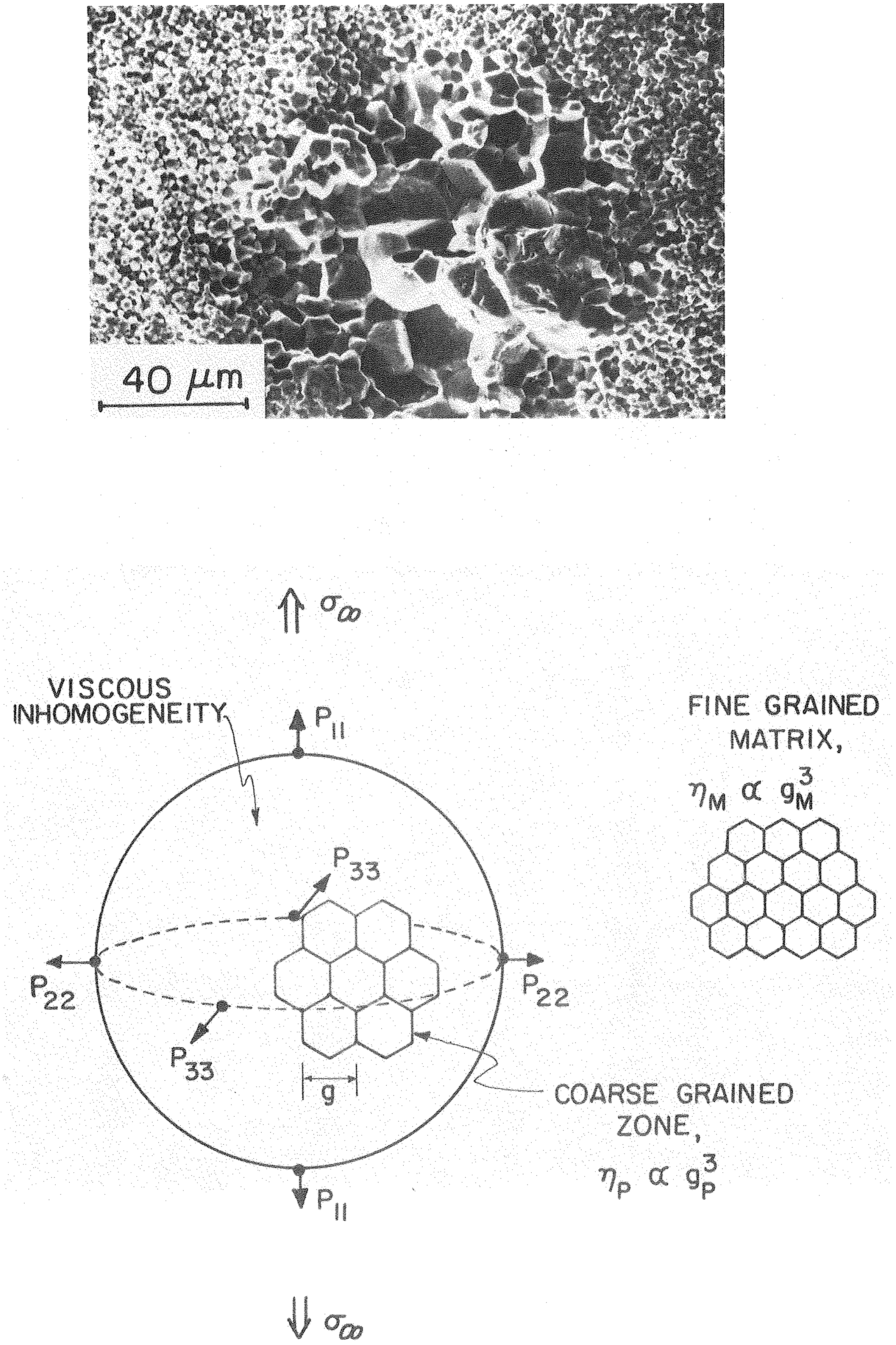

XBB814-3791

Fig. 12

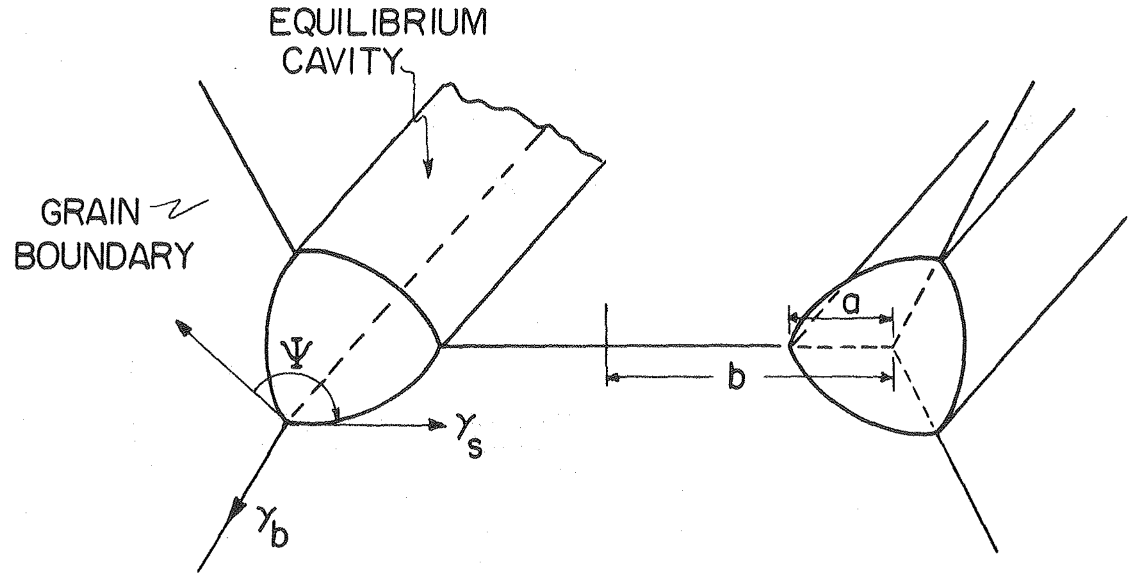

a) EQUILIBRIUM CAVITIES

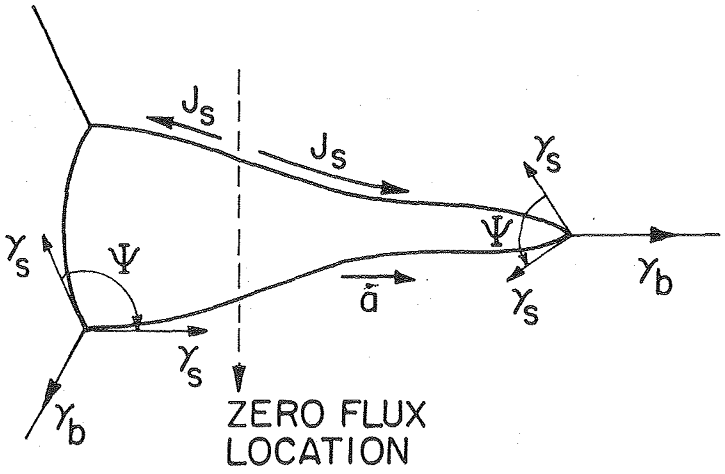

b) CRACK-LIKE CAVITY

XBL 8010-6151

Fig. 13

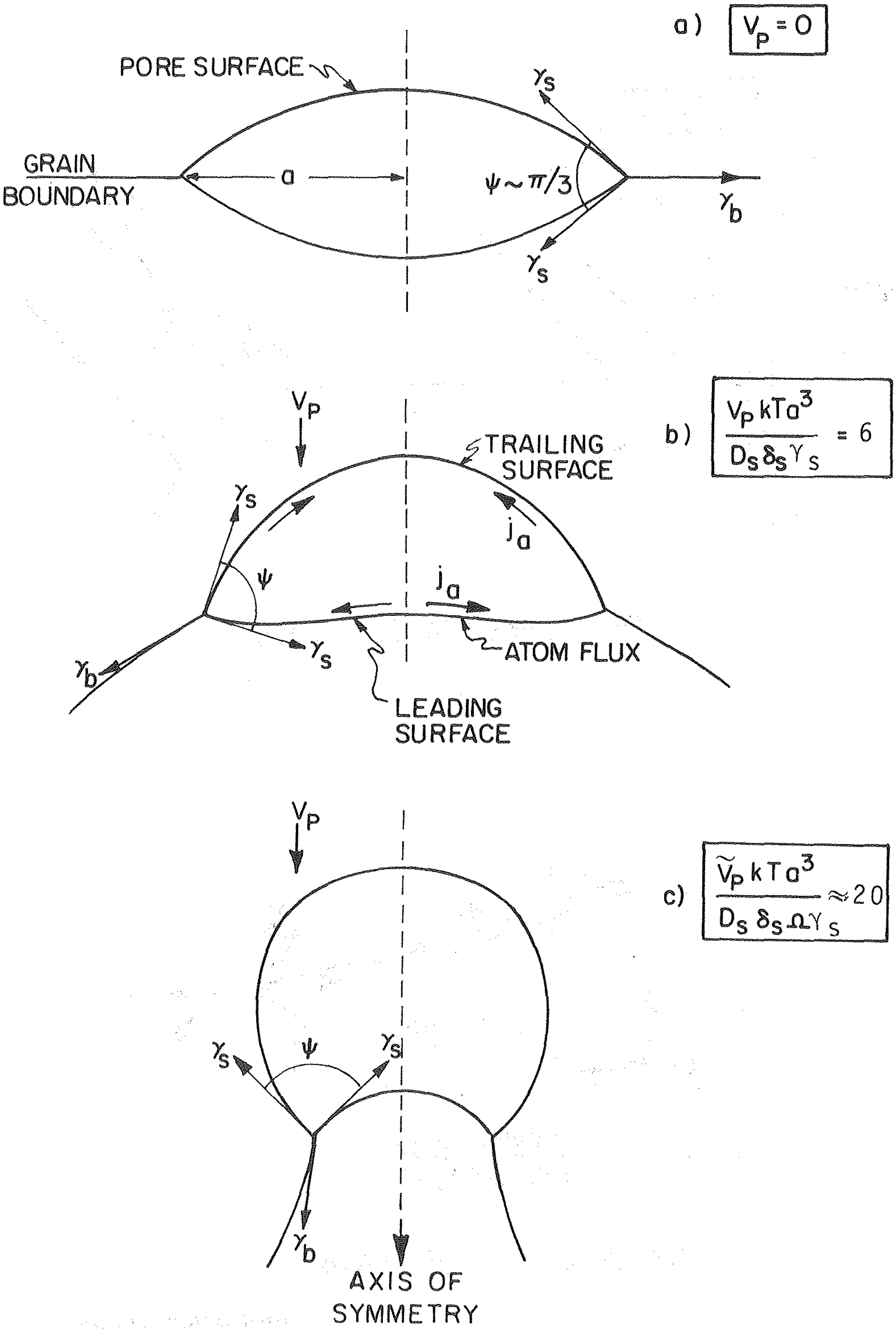

XBL 813-5418

Fig. 14

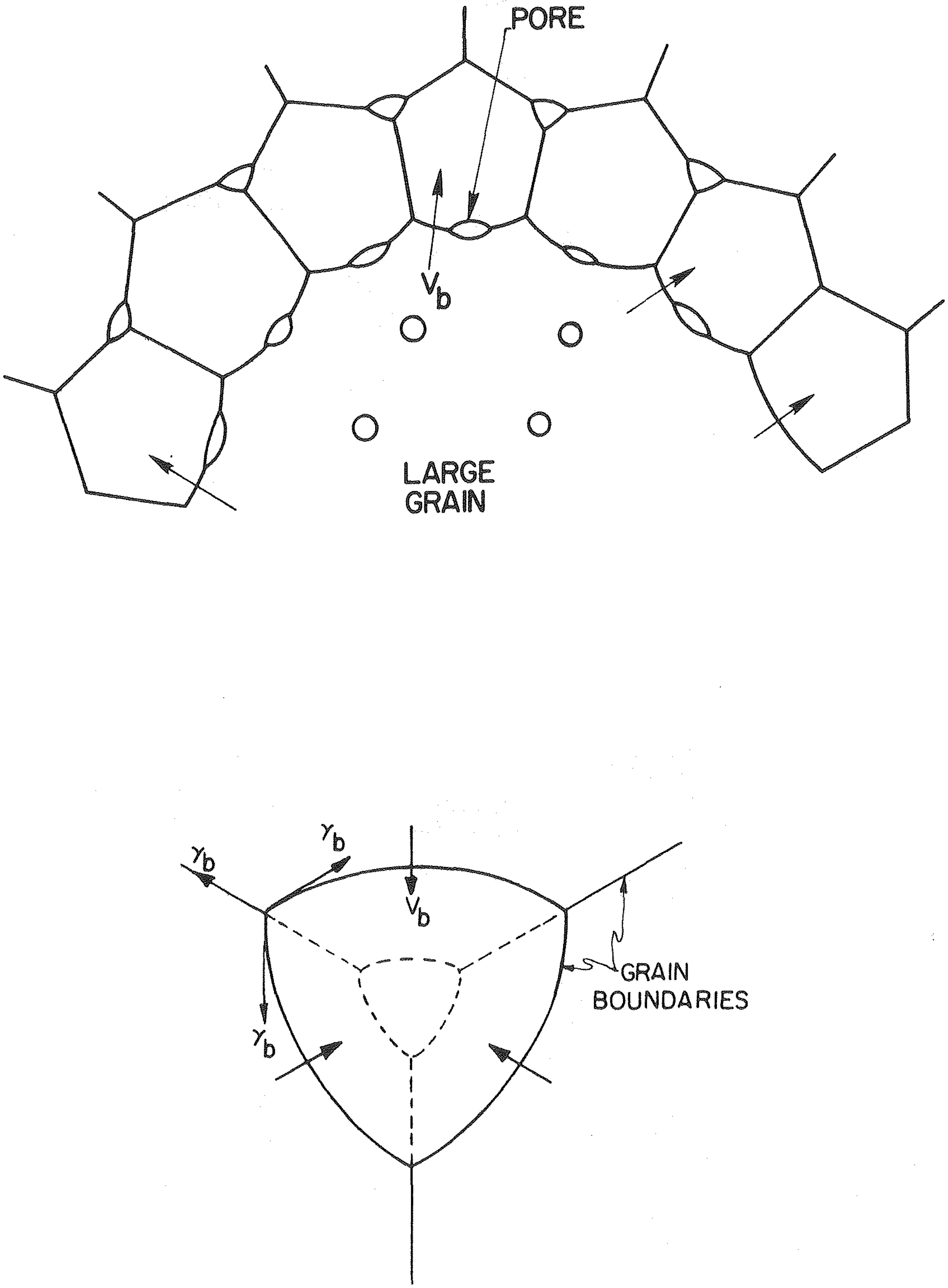

XBL 814-9385

Fig. 15

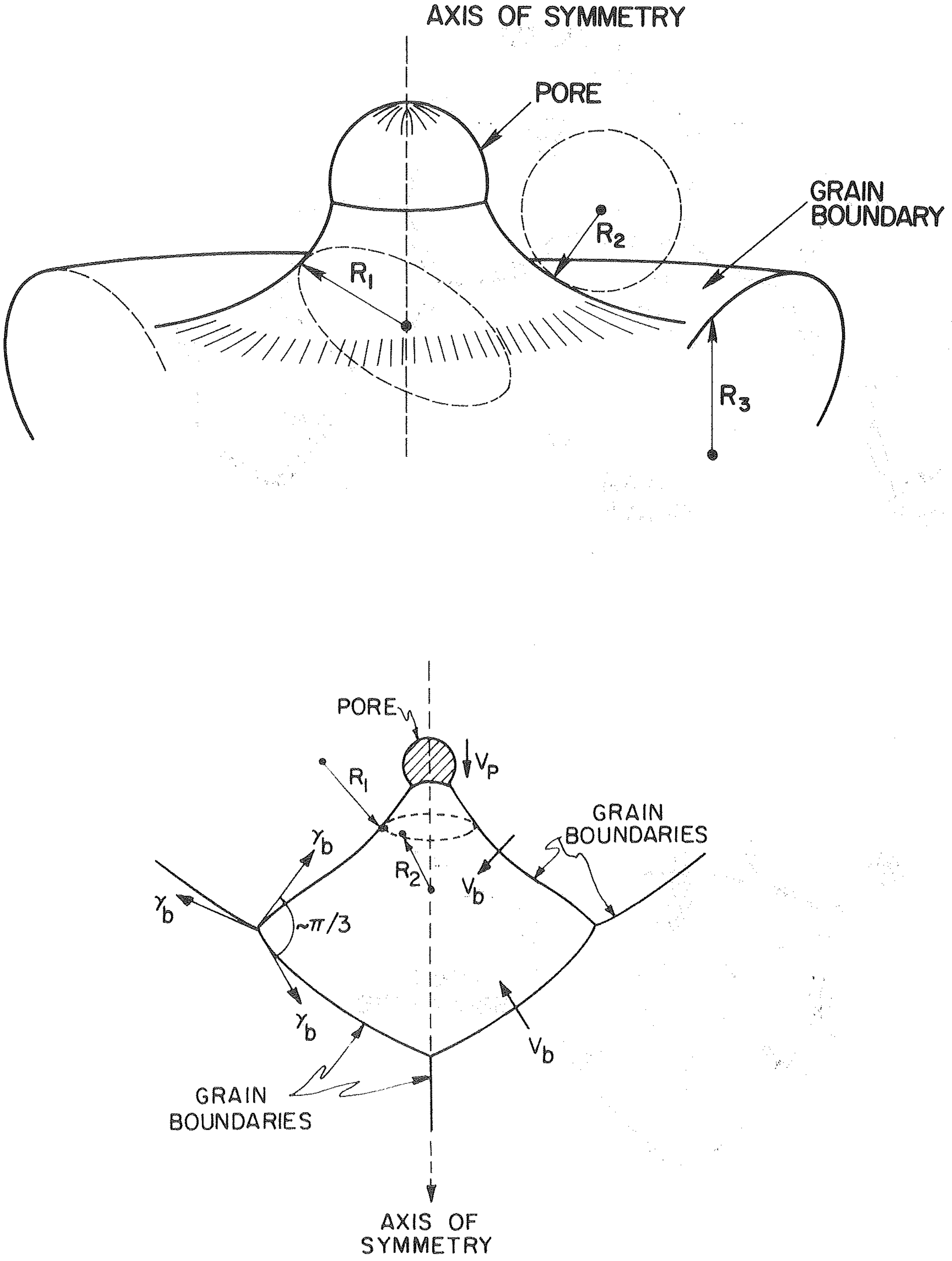

XBL 814-9384

Fig. 16

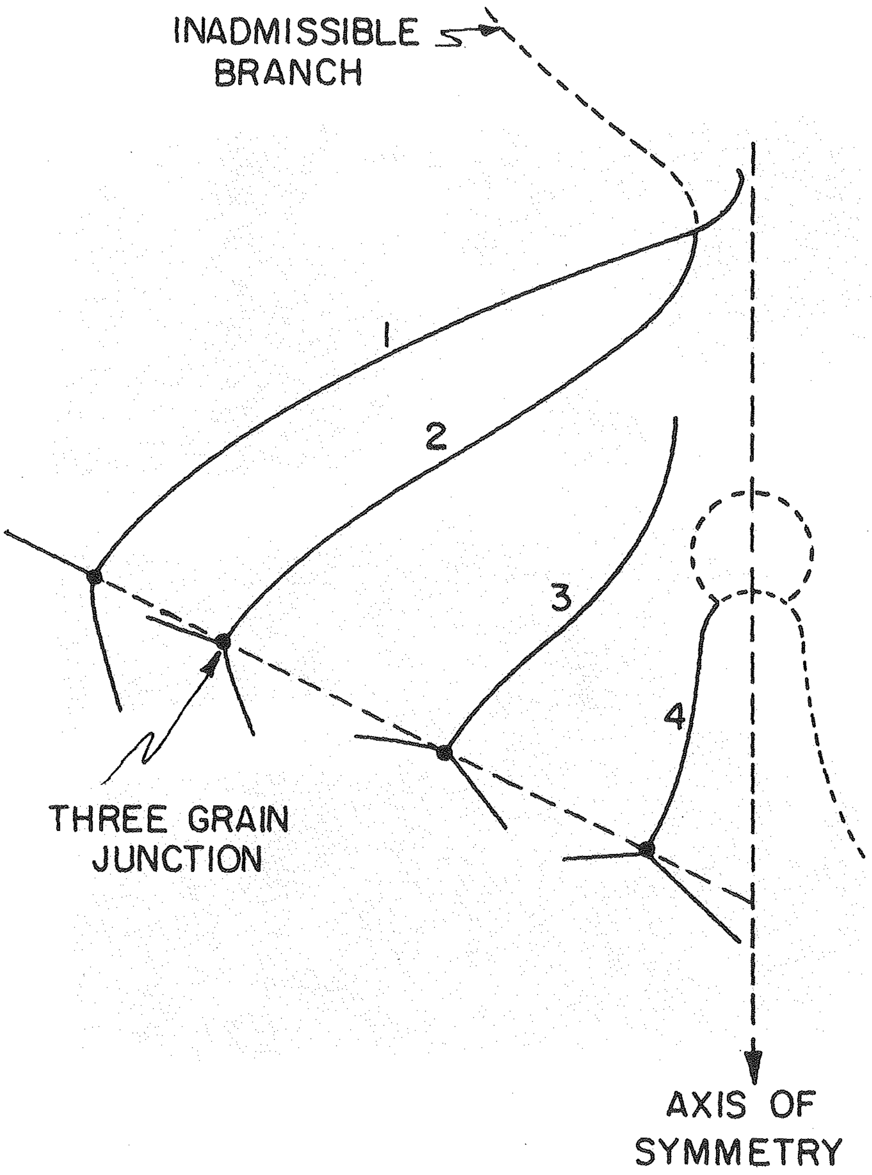

XBL 813-5420

Fig. 17

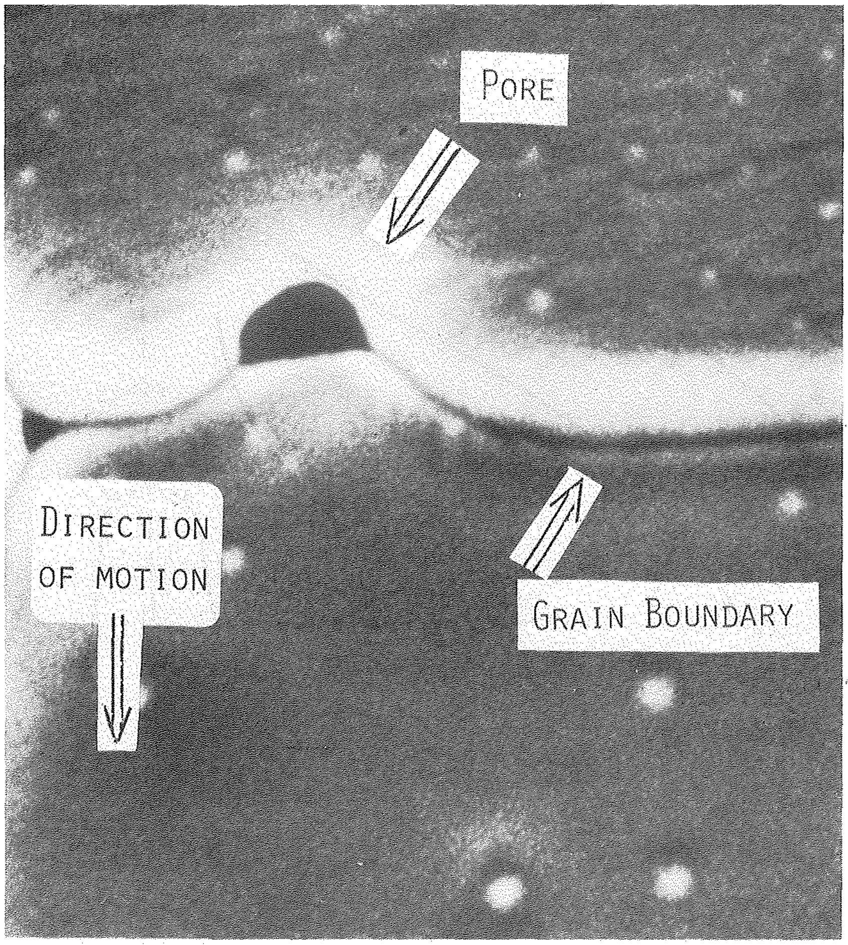

XBB814-3234A

Fig. 18

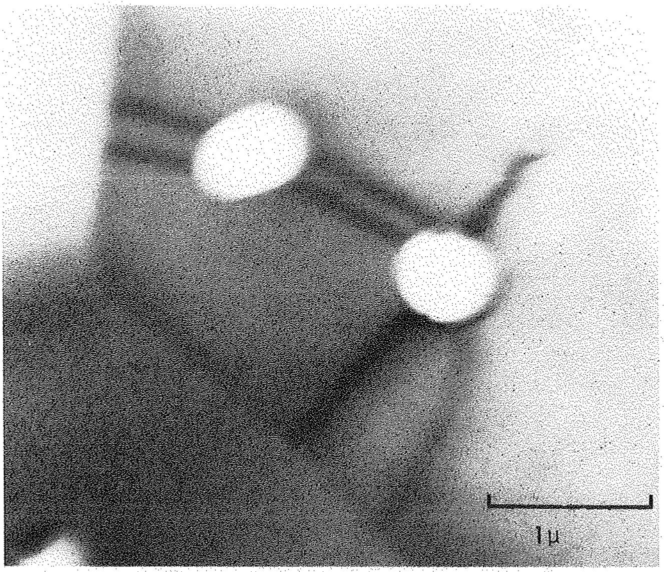

XBB8012-14682

Fig. 19a

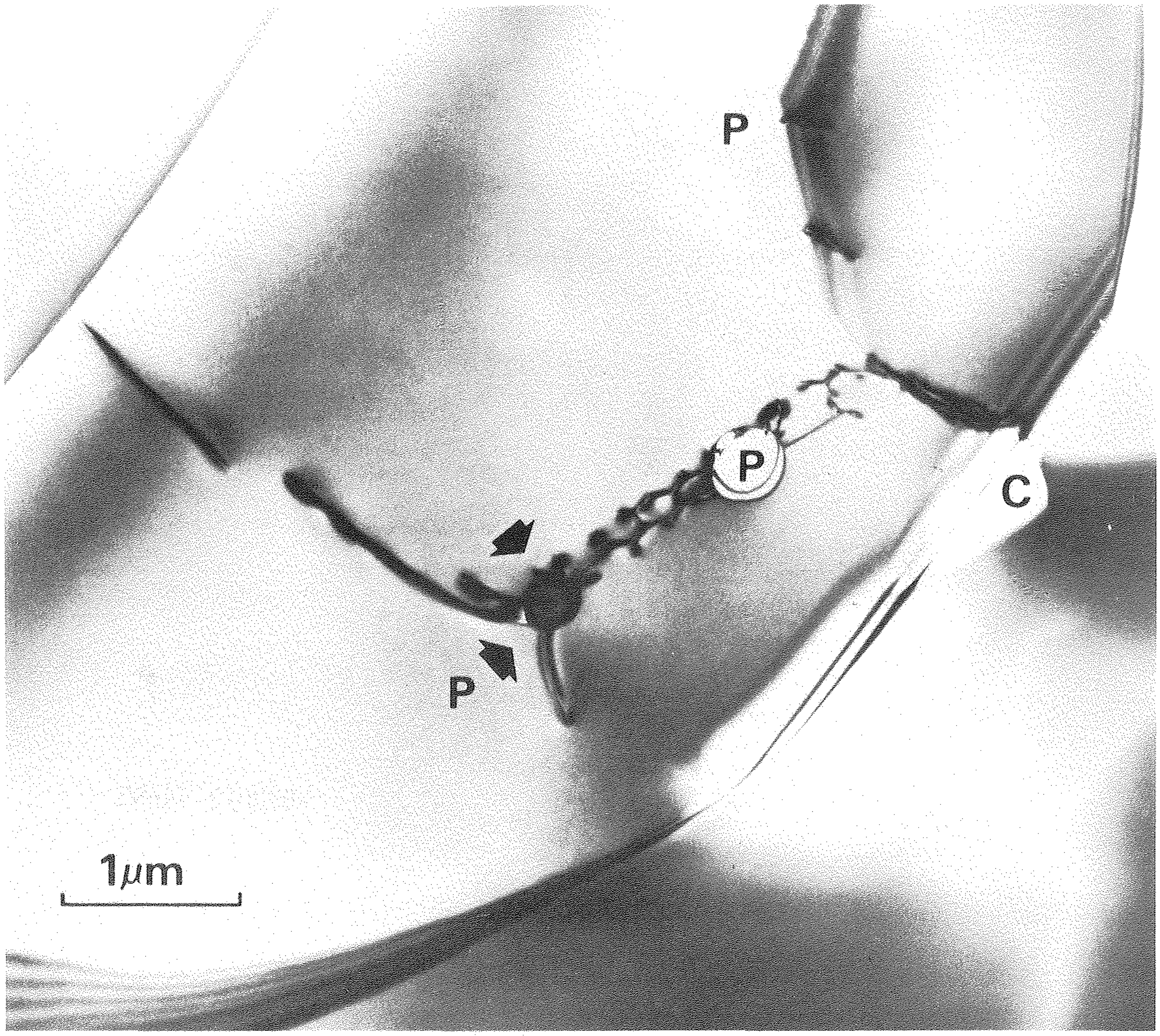

XBB817-6604

Fig. 19b

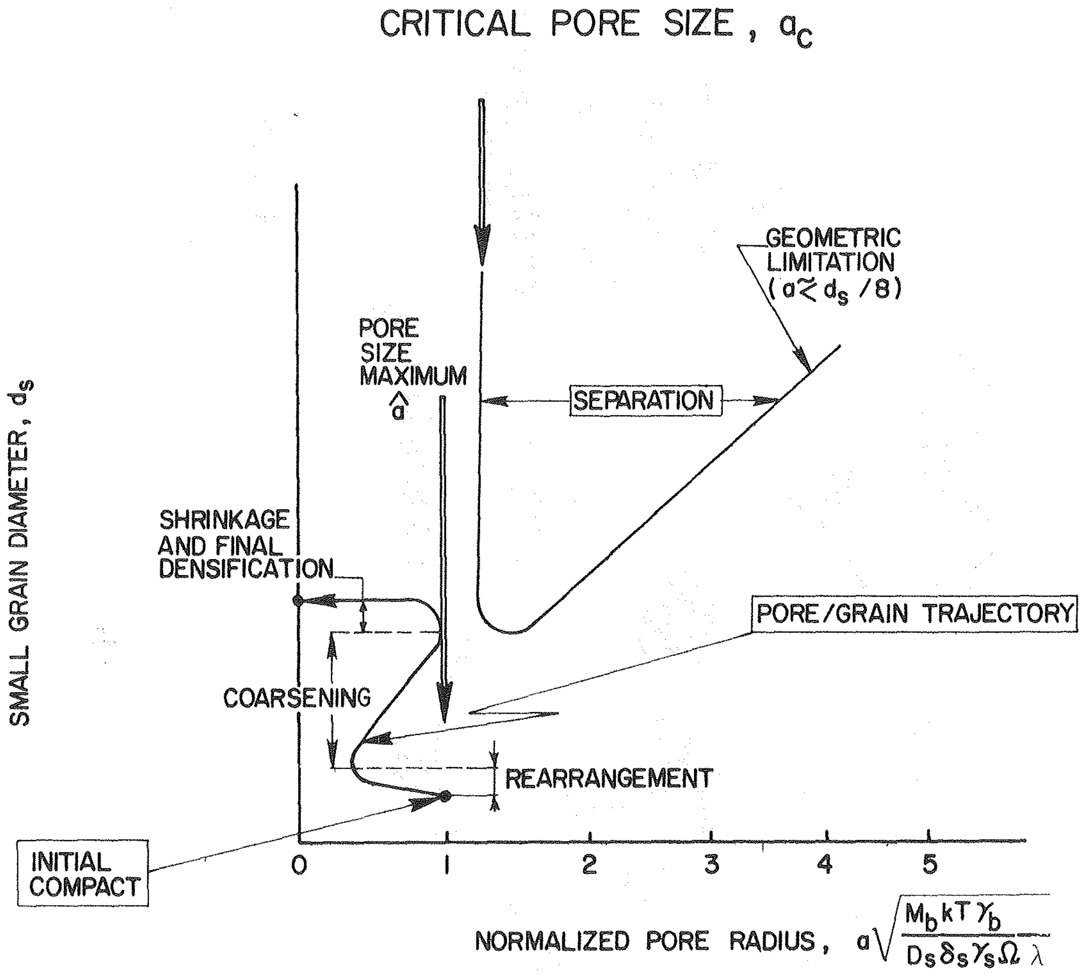

XBL 814-9441

Fig. 20

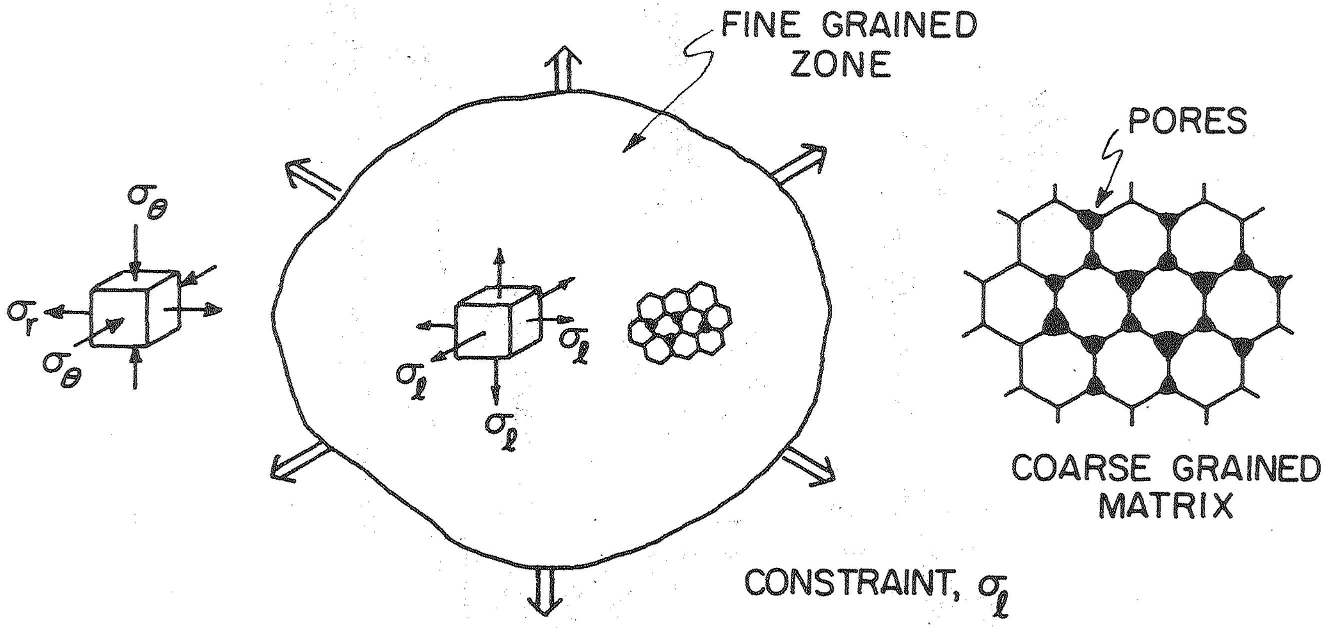

XBL 813-5422

Fig. 21